GABA-Glutamate supramammillary neurons control theta and gamma oscillations in the dentate gyrus during paradoxical (REM) sleep

Abbreviated title: SuML-dDG increases θ and γ powers during REM

Francesca Billwiller[1]*, Laura Castillo[2]*, Heba Elseedy[24]*, Anton Ivanovich Ivanov[2], Jennyfer Scapula[2], Antoine Ghestem[2], Julien Carponcy[1], Paul Antoine Libourel[1], Hélène Bras[3], Nabila ElSayed Abdelmeguid[4], Esther Krook-Magnuson[5], Ivan Soltesz[6], Christophe Bernard[2], Pierre-Hervé Luppi[1$], Monique Esclapez[2$@]
* equal contributing first authors; $ equal contributing senior authors

[1]UMR 5292 CNRS/U1028 INSERM, Centre de Recherche en Neurosciences de Lyon (CRNL), Université Claude Bernard Lyon I, LYON Cedex 08, France
[2]Aix Marseille Univ, INSERM, INS, Institut de Neurosciences de Systèmes, Marseille, France
[3] Aix Marseille Univ, CNRS, INT, Institut de Neurosciences Timone, Marseille, France
[4] Zoology Department, Faculty of Science, Alexandria University, Alexandria, Egypt
[5]Department of Neuroscience, University of Minnesota, Minneapolis, MN 55455, USA
[6]Department of Neurosurgery, Stanford University, USA

Corresponding author: Dr. Monique Esclapez
Institut de Neurosciences des Systèmes - INS
UMR 1106 INSERM - Aix-Marseille Université,
Faculté de Médecine Timone,
27 Boulevard Jean Moulin
13385 Marseille Cedex 05, France
@ monique.esclapez@univ-amu.fr

Number of pages: 54
Number of figures: 8
Number of words for:
Abstract: 249
Significant statement: 116
Introduction: 633
Discussion: 1449

Acknowledgements
This work was supported by INSERM and Aix-Marseille University (M. E, H. E., C. B., L. C., Al. I, A. G., J. S.,); Partenariats Hubert Curien (PHC) IMHOTEP (M.E., H.E., NE. A.); Agence Universitaire Francophone (H.E); CNRS, Fondation pour la recherche médicale (FRM), Societé Francaise de Recherche et Médecine du Sommeil (SFRMS), University Claude Bernard of Lyon (F.B., P-H. L., P-A. L., S. A.) and NS104590 (I. S., E. K-M).
We thank the animal facility (CEFOS, AMU, Marseille), the imaging facility (INPHIM, AMU, Marseille) and the electron microscope facility (IBDM, Marseille).

Abstract

Several studies suggest that neurons from the lateral region of the SuM (SuML) innervating the dorsal dentate gyrus (DG) display a dual GABAergic and glutamatergic transmission and are specifically activated during paradoxical (REM) sleep (PS). The objective of the present study is to fully characterize the anatomical, neurochemical and electrophysiological properties of the SuML-DG projection neurons and to determine how they control DG oscillations and neuronal activation during PS and other vigilance states. For this purpose, we combine structural connectivity techniques using neurotropic viral vectors (rabies virus, AAV), neurochemical anatomy (immunohistochemistry, in situ hybridization) and imaging (light, electron and confocal microscopy) with *in vitro* (patch clamp) and *in vivo* (LFP, EEG) optogenetic and electrophysiological recordings performed in transgenic VGLUT2-cre male mice. At the cellular level, we show that the SuML-DG neurons co-release GABA and glutamate on dentate granule cells and increase the activity of a subset of DG granule cells. At the network level, we show that activation of the SuML-DG pathway increases theta power and frequency during PS as well as gamma power during PS and waking in the DG. At the behavioral level, we show that the activation of this pathway does not change animal behavior during PS, induces awakening during slow wave sleep and increases motor activity during waking. These results suggest that the SuML-DG pathway is capable of supporting the increase of theta and gamma power in the DG observed during PS and plays an important modulatory role of DG network activity during this state.

Significant statement

An increase of theta and gamma power in the dentate gyrus (DG) is an hallmark of paradoxical (REM) sleep (PS) and is suggested to promote learning and memory consolidation by synchronizing hippocampal networks and increasing its outputs to cortical targets. However the neuronal networks involved in such control of DG activity during PS are poorly understood. The present study identifies a population of GABA/Glutamate neurons in the lateral supramammllary nucleus (SuML) innervating the DG that could support such control during PS. Indeed, we show that activation of these SuML-DG projections increase theta power and frequency as well as gamma power in the DG specifically during PS and modulate activity of a subset of DG granule cells.

Introduction

The supramammillary nucleus (SuM) is a thin structure overlying the mammillary bodies in the hypothalamus that provides substantial projections to many regions of the limbic system including the hippocampal formation (for review see Pan and McNaughton 2004, Vertes 2015). The SuM is composed of several populations of neurons that differ in their neurochemical content and the specificity of their connections (Swanson et al., 1982; Gonzalo-Ruiz et al., 1992; Leranth and Kiss, 1996; Kocsis et al., 2003; Borhegyi and Leranth, 1997; Haglund et al., 1984). In rats, many studies have described the projections from SuM neurons to the hippocampus (Segal & Landis, 1974; Pasquier & Reinoso-Suarez, 1976, 1978; Wyss et al., 1979; Haglund et al., 1984; Saper et al., 1985; Vertes, 1992; Magloczky et al., 1994; Nitsch and Leranth 1996; Vertes & McKenna, 2000). We (Soussi et al., 2010) and others (Boulland et al., 2009) demonstrated in rats that SuM neurons from the most medial part of the SuM (SuMM; Paxinos and Watson, 1998), referred as SuMm by Swanson (1998), or SuMp by Pan and McNaughton (2004) innervating the inner molecular layer of the ventral dentate gyrus (DG) and CA2 pyramidal cells are glutamatergic (Soussi et al., 2010). In contrast, SuM neurons located in the lateral two-third region of the SuM (SuML), referred as SuMg by Pan and McNaughton (2004), innervate the supragranular layer of the dorsal DG (dDG) and to a lesser extend the ventral DG (vDG) and display a unique dual glutamatergic and GABAergic neurotransmitter phenotype (Boulland et al., 2009; Soussi et al., 2010). Indeed, these SuML neurons and their projections to the dDG co-express markers for both glutamatergic (vesicular glutamate transporter 2; VGLUT2) and GABAergic (glutamate decarboxylase 65, GAD65 and vesicular GABA transporter,

98 VGAT) neurotransmission and establish asymmetric and symmetric synapses on DG
99 cells (Soussi et al., 2010). The connectivity and neurochemical properties of these
100 different SuM-hippocampal pathways suggest that they may contribute differently to
101 hippocampal dependent functions. Indeed, it has been shown that the SuM controls
102 hippocampal theta rhythm (Kocsis and Vertes 1994, Vertes and Kocsis 1997, Kocsis
103 and Kaminski 2006) and is involved in emotional learning and memory (Pasquier and
104 Reinoso-Suarez 1976, Richmond et al 1999, Pan and McNaughton 2002, Santin et al
105 2003, Pan and McNaughton 2004, Shahidi et al. al., 2004). By combining retrograde
106 tracing, neurotoxic lesion and FOS immunostaining, it was recently shown that SuML
107 GABA/Glutamate neurons are responsible for the activation of dDG granule cells during
108 paradoxical sleep (PS) (Renouard et al., 2015 ; Billwiller et al., 2016). Such activation
109 may play a key role in the previously reported beneficial effect of PS on learning and
110 memory (Maquet et al., 2000). In addition, Pedersen and colleagues (2017), by using a
111 chemogenetic approach in transgenic mice, showed that SuM neurons containing only
112 VGLUT2 but not those containing VGAT and VGLUT2 play a crucial role in waking.
113 Altogether these results suggest that glutamatergic neurons from the SuM known to
114 innervate several limbic regions including the CA2/CA3a hippocampal region and the
115 vDG are involved in normal wakefulness whereas the GABA/Glutamate SuML neurons
116 projecting to the dDG could be instrumental for PS function.
117 In this study we investigate how the SuML-dDG pathway control dDG neurons activity
118 during PS and other vigilance states. For this purpose we combine innovative structural
119 connectivity techniques using neurotropic viral vectors (rabies virus, AAV),
120 neurochemical anatomy (immunohistochemistry, *in situ* hybridization) and imaging (light,
121 electron and confocal microscopy) with *in vitro* (patch clamp) and *in vivo* (LFP, EEG)

optogenetic and electrophysiological recordings performed in transgenic VGLUT2-cre mice in order: 1) to fully characterize the anatomical, neurochemical and electrophysiological properties of the SuML-dDG projection neurons in our mice trangenic model and 2) to determine the influences of this specific pathway on behaviors and associated oscillatory activities characterizing the different vigilance states as well as DG neuron activity.

128 ## Materials and methods

129 ### Animals

130 For this study, we used 26 transgenic “VGLUT2-cre” adult male mice (25-30 g; aged 10-
131 11 weeks) obtained by mating male and female homozygote Vglut2-ires-Cre mice from
132 Jackson Laboratories (Strain name Slc17a6$^{tm2(cre)Lowl}$/J, stock #016963). All mice were
133 bred in-house and maintained in standard cages, with food and water *ad libitum*, in a
134 temperature- and humidity-controlled room under a 12 hr light/12 hr dark cycle. All the
135 surgical and experimental procedures were performed according to the National
136 Institutes of Health guidelines and the European communities Council Directive of
137 86/609/EEC and were approved by the University of Aix-Marseille and Lyon University
138 Chancellor's Animal Research Committees.

139

140 ### Vectors

141 ***Rabies virus***

142 Four VGLUT2-cre mice underwent stereotaxic injection of rabies virus (RV) within the
143 inner molecular layer of the dDG in order to obtain golgi-like retrograde-labeling of SuM
144 neurons projecting to this region. The strain of RV used was the Challenge Virus
145 Standard (CVS, 4.10^7 plaque-forming units/mL) (Bras et al. 2008; Ugolini 2010; Coulon
146 et al. 2011). Only vaccinated personnels conducted these experiments at the
147 appropriate biosafety containment level until the sacrifice of the animals as described
148 below.

149 These animals were used to determine the neurotransmiter phenotype of SuM neurons
150 projecting to dDG at the mRNA level, combining immunohistofluorescent detection of RV

151 with fluorescent *in situ* hybridization detection of VGAT and VGLUT2 mRNAs.

152 ***Adeno-Associated Virus (AAV) Double floxed Inverted ORF (DIO) vectors***

153 Thirteen VGLUT2-cre mice underwent stereotaxic injection of the cre-dependent viral
154 vectors: AAV5-EF1a-DIO-EYFP (3.5 10^{12} virus molecules / ml; UNC Gene Therapy
155 Center Vector Core; Dr Deisseroth) into the SuML. These VGLUT2-EYFP mice
156 expressing the Yellow Fluorescent Protein (YFP) in VGLUT2 SuM neurons and their
157 axon terminals were used 1) to determine the neurotransmitter phenotype of SuM
158 neurons innervating the dDG at the protein level, by simultaneous
159 immunohistofluorescent detection of EYFP labeled axon fibers and terminals, VGAT and
160 VGLUT2 in dDG (n=3); 2) to determine the synaptic profile of these EYFP labeled axon
161 terminals at the electron microscopy level (n=3); 3) as control animals (n=3) for *in vitro*
162 optogenetic stimulation and patch clamp electrophysiological recordings; 4) as control
163 animals (n=4) for *in vivo* optogenetic stimulation and electrophysiological recordings
164 followed by cFos immunolabeling.

165 Nine VGLUT2-cre mice underwent stereotaxic injection of the cre-dependent viral
166 vectors: AAV5-EF1a-DIO-hChR2(H134R)-EYFP (3.2 10^{12} virus molecules / ml; UNC
167 Gene Therapy Center Vector Core; Dr. Deisseroth) into the SuML. These VGLUT2-
168 ChR2 mice expressing the excitatory opsin, channelrhodopsine 2 (ChR2) and the
169 reporter protein EYFP in VGLUT2 SuM neurons and their axon terminals were used for
170 1) *in vitro* optogenetic stimulation and patch clamp electrophysiological recordings
171 experiments (n=5); 2) *in vivo* optogenetic stimulation and electrophysiological recordings
172 followed by cFos immunolabeling (n=4).

173

174 **Surgery**

175 Mice were anesthetized by an intraperitoneal injection (i.p.) of Ketamin (50mg/kg) /
176 Xylazine (5mg/kg) solution. If necessary, this anesthesia was repeated during the
177 surgery. Animals were then secured in a stereotaxic frame (David Kopf instruments).
178 The body temperature of mice was monitored and maintained at about 37°C during the
179 entire procedure by means of an anal probe and heating blanket respectively. The head
180 was shaved and sanitized with Betadine and 0.9% NaCl. Local anesthesia was
181 performed by infiltration of the scalp with xylocaine (lidocaine hydrochloride 0,5%), and
182 an ophthalmic gel was placed on the eyes to avoid drying. After scalp incision, holes
183 were drilled in the skull, with antero-posterior (AP), medio-lateral (ML) and dorso-ventral
184 (DV) coordinates based on Paxinos & Franklin's atlas (2005).

185 ***RV and AAV viral vector injections***

186 The RV (200 nl) was pressure-injected unilaterally (n=2) or bilaterally (n=2) within the
187 dDG inner molecular layer of VGLUT2-cre mice according to the following coordinates:
188 AP = -2; ML = +/-1.5; DV = -1.7. Injections were performed by using a 33-gauge
189 Hamilton syringe connected to a Micro4 injection pump system (World Precision
190 Instruments). After completion of the injection procedures, the syringe was removed and
191 the skin was sutured. Animals were treated with local anesthetic, returned to their cages
192 kept at the appropriate biosafety containment level for a survival period of 38h to
193 observe an optimal RV retrograde labeling for the dendritic arbor of SuM neurons.
194 AAV5-EF1a-DIO viral vectors (500nl) were injected bilaterally within the SuML of
195 VGLUT2-cre mice at the following coordinates: AP = -2.7; LM = +/-1.25; DV = -4.8 using
196 an 11°angle to avoid the high vascularization at the midline.

197

198 ***Optrode and electrode implantation***

199 After AAV injections, VGLUT2-mice were implanted with an optrode in the left dDG (AP
200 = -2; ML = -1.1; DV = -1.7) for optic stimulation of axon terminals originating from
201 transfected SuML neurons and local field potential (LFP) recordings from the DG. The
202 optrode consisted of an optic fiber (250 μm ∅, 0.39 NA; Thorlabs SAS) and the LFP
203 electrode. The LFP electrodes consisted of two 45 μm diameter tungsten wires
204 (California Fire Wire Company), twisted and glued together to form a rigid and solid
205 structure, with the 2 ends of the wires separated by 100 μm from each other. Two small
206 screws (1 mm in diameter, Plastics One) each soldered to a wire were fixed on the skull.
207 The first screw was fixed in the parietal part of the skull for EEG recording; the second
208 screw, at the level of cerebellum as reference electrode. Two wire electrodes were
209 inserted into the neck muscles for bipolar EMG recordings. All leads were connected to
210 a miniature plug (Plastics One) that was cemented on the skull.

211 After completion of the surgery the skin was sutured. Mice were treated with local
212 anesthetic, and an intramuscular injection of antibiotic (Baytril, 5mg/kg) to prevent any
213 risk of infection. Mice were monitored until waking and replaced in their home cages for
214 a survival period of 3 weeks.

215

216 **Histology**

217 ***Tissue preparation for light microscopy***

218 Animals were deeply anesthetized with ketamine and xylazine and transcardially
219 perfused with 4% paraformaldehyde (PFA) in 0.12 M sodium phosphate buffer, pH 7.4
220 (PB). After perfusion, the brains were removed from the skull, post-fixed in the same
221 fixative for 1 h at room temperature (RT), rinsed in PB, cryoprotected in 20% sucrose

222 overnight, frozen on dry ice and sectioned coronally at 40 µm with a cryostat (Microm).
223 The sections were rinsed in PB, collected sequentially in tubes containing an ethylene
224 glycol-based cryoprotective solution and stored at -20°C until histological processing.
225 One of every ten sections was stained with cresyl violet to determine the general
226 histological characteristics of the tissue throughout the rostro-caudal extent of the brain.
227 Selected sections were processed for 1) simultaneous detection of VGLUT2 mRNA,
228 VGAT mRNA and RV; 2) simultaneous immunohistofluorescent detection of EYFP,
229 VGLUT2 and GAD65 or VGAT; 3) immunohistochemical detection of cFos.

230 ***Simultaneous detection of VGLUT2 mRNA, VGAT mRNA and RV combining***
231 ***fluorescent in situ hybridization (RNAscope technology) and***
232 ***immonhistofluorescent methods performed in VGLUT2-cre mice injected with RV***

233 Selected sections at the level of the SuM were first treated with 1% H2O2 rinsed in PB
234 mounted on SuperFrost Plus slides (Fisher Scientific) and air dried at RT. They were
235 then processed for fluorescent RNAscope *in situ* hybridization according to the
236 manufacter's protocol (Advanced Cell Diagnostics). Briefly sections were treated with
237 100% ethanol and protease III for 30 min at 40°C. They were incubated in a solution
238 containing both RNAscope® Probe - Mm-S1c17a6 for detection of VGLUT2 mRNA and
239 Mm-S1c32a1-C3 for detection of VGAT mRNA. After hybridization, sections were then
240 processed for visualization using the RNA-scope Multiplex Fluorescent reagent Kit v2
241 (Advanced Cell Diagnostics) and the Tyramide Signal Amplification (TSA™) Plus
242 Cyanine 3 and TSA Plus Cyanine 5 systems (Perkin Elmer).

243 After the RNAscope assay, sections were rinsed in 0.02 M potassium phosphate-
244 buffered saline (KPBS, pH 7.2-7.4) and processed for immnohistofluorescent detection
245 of the RV using a Mouse On Mouse kit (MOM, Vector Laboratory) to eliminate non

246 specific labeling due to use of mouse monoclonal antibody on mouse tissue. Sections
247 were incubated for 1 h at RT in MOM mouse IgG blocking reagent diluted in KPBS
248 containing 0.3% Triton X-100. Sections were rinsed twice with KPBS for 5 min and pre-
249 incubated in MOM diluent for 15 min. Sections were then incubated overnight at RT in a
250 solution containing the mouse monoclonal antibody directed against RV (1:3000; Raux
251 et al., 1997 Kindling provided By Dr. Patrice Coulon), diluted in MOM diluent. After
252 several rinses in KPBS, they were incubated for 2 h in Alexa488-conjugated donkey
253 anti-mouse (1:200; Invitrogen) diluted in MOM diluent. After several rinses in KPBS, all
254 sections were coverslipped with Fluoromount (Electron Microscopy Sciences). The
255 specimens were analyzed with a Zeiss laser-scanning confocal microscope.

256 ***Quantification of co-localizing RV, VGLUT2 and VGAT mRNAs***

257 Quantitative analysis was conducted to evaluate the extent of SuM neurons with direct
258 projections to the dDG that co-express VGLUT2 and VGAT mRNAs. For this purpose,
259 the number of triple neurons was determined for each animal (n=4), from 3 sections
260 (120 μm apart from each other) across the antero-posterior extent of the SuM. For each
261 section, an image of the entire SuM region was obtained from a single confocal slice
262 using the Tile Scan function with a 20x objective and sequential acquisition of the
263 different wavelength channels to avoid fluorescent talk with ZEN software (Zeiss). The
264 analysis was then performed with Neurolucida software (version 7, mbfBioscience) as
265 follows: for each confocal image, all RV- labeled neurons were identified on the green
266 channels and examined for colocalization of VGLUT2 mRNA in the blue channel and/or
267 VGAT mRNA in the red one. Triple- double- and single-labeled neurons were tagged
268 differently and counted by the software. A total of 380 RV-labeled neurons were
269 analyzed.

270 ***Simultaneous immunohistofluorescent detection of EYFP, VGLUT2 and GAD65 or***
271 ***VGAT performed in VGLUT2-EYFP mice***

272 Selected sections at the level of the dDG were processed using the MOM kit as
273 described above. Sections were incubated overnight at RT in a solution containing rabbit
274 anti-GFP (1:2000, Invitrogen), guinea pig anti-VGLUT2 (1:5000, Millipore) and mouse
275 anti-GAD65 (1:100, Millipore) or mouse anti-GFP (1:100, Invitrogen), guinea pig anti-
276 VGLUT2 (1:5000, Millipore) and rabbit anti-VGAT (1:1000, Synaptic System) diluted in
277 MOM diluent. After several rinses in KPBS, they were incubated for 2 h in Alexa488-
278 conjugated donkey anti-rabbit IgG (1:200; Invitrogen), Cy5-conjugated donkey anti-
279 guinea pig (1:100; Jackson ImmunoResearch Laboratories, Inc.), and Cy3-conjugated
280 donkey anti-mouse (1:100; Jackson ImmunoResearch Laboratories, Inc.) or Alexa488-
281 conjugated donkey anti-mouse IgG (1:200; Invitrogen), Cy5-conjugated donkey anti-
282 guinea pig (1:100; Jackson ImmunoResearch Laboratories, Inc.), and Cy3-conjugated
283 donkey anti-rabbit (1:100; Jackson ImmunoResearch Laboratories, Inc.) diluted in MOM
284 diluent. After several rinses in KPBS, all sections were then mounted on superfrost-
285 coated slides, dried overnight at RT and coverslipped with Fluoromount. The specimens
286 were analyzed with confocal microscope (Zeiss).

287 ***Quantification of co-localizing GFP, VGLUT2 and VGAT***

288 Two quantification protocols were used in order to evaluate the extent of the different
289 neurochemical phenotypes of axon terminals from the SuM innervating the dDG. In the
290 first protocol previously described (Soussi et al., 2015), the densities of VGLUT2/VGAT
291 and VGLUT2 only labeled terminals were assessed by the quantification of
292 immunolabeling for VGLUT2/VGAT and VGLUT2 only, respectively. These analyses
293 were performed on 4 sections for each mouse. Single optical confocal images were

294 acquired with Zeiss LSM 510 laser-scanning microscope and analyzed with the software
295 provided by the microscope manufacturer (LSM 510 Zen, Zeiss). All images were
296 acquired from the suprapyramidal and infrapyramidal blades of the dDG, using identical
297 parameters. The percentages of VGLUT2 labeled terminals containing VGAT were
298 estimated by the the Manders' coefficient (proportion of pixels for VGLUT2 also positive
299 for VGAT) obtained with the JACoP co-localization Plugin for Image J, in the region of
300 interest (ROI) which included granule cell layer (GCL) and the narrow zone superficial
301 to the granule cells defined as the supragranular layer (SGL) following recommendations
302 from Bolte & Cordelières (2006). For each channel, an identical bottom threshold was
303 applied throughout the analyses, and only the pixels with a value above this threshold
304 were counted. When a pixel had a value above the threshold in both channels, it was
305 counted as double positive. The size and the shape of the ROI was the same for each
306 confocal image. The average % of co-localization was calculated for each blade of the
307 DG for each mouse.
308 In the second quantification protocol, we determined for each mouse (n=4), the relative
309 percentages of triple- and double-labeled boutons for the GFP anterograde tracer and
310 VGAT and／or VGLUT2 in the SGL and infragranular blade of the dDG from several z-
311 stacks of 10 confocal slices, acquired with the 100X objective and a numerical zoom 8,
312 in three different sections. The analysis was performed as previously described
313 (Persson et al., 2006; Soussi et al., 2010) and following recommendations from Bolte &
314 Cordelières (2006). For each z-stack, the confocal images obtained from separate
315 wavelength channels (green, red and blue) were displayed side by side on the computer
316 screen together with the images corresponding to colocalized pixels within each optical
317 slice of the z-stack obtained with the colocalization highlighter plugin in ImageJ. The

318 GFP-labeled boutons were identified in the green channel within a probe volume defined
319 by the size of the confocal slice (19.38 μm · 19.38 μm) and the height of the z-stack (2
320 μm). Each bouton was examined for colocalization through the individual optical slices of
321 the z-stack. Single-, double- and triple-labeled boutons were counted using the Cell
322 Counter plugin in Image J. The total number of GFP-labeled terminals analyzed in the
323 two regions of interest was 400.

324 ***Immunohistochemical detection of cFos performed in VGLUT2-EYFP (n=4) and***
325 ***VGLUT2-ChR2 (n=4) mice***

326 Selected sections at the level of the DG were processed for immunohistochemistry
327 according to previously described protocol (Esclapez et al. 1994). Sections were pre-
328 treated for 30 min in 1 % H2O2, rinsed in PB and KPBS, preincubated for 1 h in 3 %
329 normal goat serum (NGS, Vector Laboratories) diluted in KPBS containing 0.3 % Triton
330 X-100 and incubated overnight at RT in cFos rabbit polyclonal antiserum (1:20,000;
331 Calbiochem) diluted in KPBS containing 1 % NGS and 0.3 % Triton X-100. After several
332 rinses in KPBS, sections were incubated for 1 h at RT in biotinylated goat anti-rabbit
333 immunoglobulin G (IgG; Vector Laboratories) diluted 1:200 in KPBS containing 3 % NGS
334 and then for 1 h at RT in an avidin-biotin-peroxidase complex solution prepared in KPBS
335 according to the manufacturer's recommendations (Vectastain ABC kit, Vector
336 Laboratories). Sections from VGLUT2-EYFP and VGLUT2-ChR2 mice were processed
337 In parallel and for the same period of time (15 min) in 3.3'-diaminobenzidine
338 tetrahydrochloride (DAB, Sigma fast tablets; Sigma), rinsed in KPBS, mounted onto
339 Superfrost Plus slides, dehydrated and coverslipped with Permount.

340

341 ***Quantification of cFos immunolabeled neurons***

342 The number of cFos labeled neurons was calculated in the DG GCL of the right and left
343 (ipsilateral to the optic stimulation) hemispheres in VGLUT2-EYFP control (n=4), and
344 VGLUT2-ChR2 (n=4) mice. These analyses were performed using a computer-assisted
345 system connected to a Nikon 90i microscope and the Neurolucida software
346 (MicroBrightField). A total of 4 sections (400 µm apart from each other) surrounding the
347 optrode site were analyzed for each animal. In each section the GCL was delineated
348 and all neurons labeled for cFos were plotted. The software calculated the total number
349 of labeled neurons in each hemisphere for each animal. The average total number of
350 labeled neurons / hemisphere ± SEM was calculated for each group of control VGLUT2-
351 EYFP and VGLUT2-ChR2 mice. Statistical analysis was performed by Statview software
352 using Wilcoxon Rank Sum Test.

353 ***Tissue preparation for electron microscopy***

354 Three VGLUT2-EYFP mice were perfused intracardially with a fixative solution
355 containing 4% PFA and 0.1% glutaraldehyde in 0.12 m PB. After perfusion, the brain
356 was removed from the skull, post-fixed in the same fixative overnight at 4°C and rinsed
357 in PB for 1.5 h. Blocks of the forebrain were sectioned coronally at 60 µm with a
358 vibratome. Pre-embedding immunolabeling for GFP sections at the level of dDG were
359 pre-treated for 15 min in 1% sodium borohydride prepared in PB and rinsed for 30 min in
360 PB and 3 x 30 min in KPBS. Sections were incubated for 1h in normal goat serum
361 diluted in 0.02M KPBS, then incubated overnight in primary antibody rabbit anti-GFP
362 (1:2000) diluted in KPBS containing normal goat serum at RT. On the following day
363 sections were rinsed for 1.5 h in 0.02M KPBS then incubated for 1h in the secondary
364 antibody goat anti-rabbit (1:200) diluted in KPBS containing normal goat serum. After

365 rinsing in KPBS for 1.5 h, sections were incubated for 1h in an avidin-biotinylated-
366 peroxidase complex (ABC Elite; Vector Laboratories) prepared in KPBS. After 3 x 30
367 min rinses in KPBS, sections were incubated for 12 min in 3.3'-diaminobenzidine
368 tetrahydrochloride and 0.01% H2O2, rinses in KPBS, post-fixed in 2% PFA and
369 2.5% Glutaraldahyde diluted in PB for 3 h, then washed for 1.5 h in PB. After all these
370 steps, sections were treated with 1% osmium tetroxide in PB for 45 min, dehydrated in
371 ethanol, flat embedded in Durcupan resin and polymerized at 56°C for 24 h (Zhang &
372 Houser, 1999). Labeled regions of the DG that contained the molecular and granule cell
373 layers were trimmed from the sections, re-embedded on capsules filled
374 with polymerized Durcupan and further polymerized at 56°C for an additional 24 h.
375 Ultrathin sections from the most superficial face of the blocks were cut on an
376 ultramicrotome. Serial sections were picked up on nickel mesh grids and stained with
377 uranyl acetate and lead citrate. Sections were examined and photographed with a JEOL
378 electron microscope.
379

380 ***In vitro* electrophysiology: optic stimulation and patch clamp recordings**

381 ***Hippocampal slice preparation***

382 VGLUT2-ChR2-EYFP mice (n=5) and VGLUT2-EYFP mice (n=3) were decapitated
383 under isofluorane anesthesia. Brains were quickly removed and placed into an ice-cold
384 (4°C) cutting solution containing (in mM): 140 potassium gluconate, 10 HEPES, 15
385 sodium gluconate, 0.2 EGTA, 4 NaCl (pH 7.2). Coronal slices were cut (350 µm) using a
386 vibratome (Leica Microsystem). In order to increase cell survival over time in slices from
387 10 to 11 week-old adult, slices were incubated first in a solution containing (in mM): 110
388 choline chloride; 2.5 KCl; 1.25 NaH_2PO_4; 10 $MgCl_2$, 0.5 $CaCl_2$; 25 $NaHCO_3$; 10 glucose,

389 5 sodium pyruvate, for 15 min at 20-23°C. Then, they were transferred to a holding
390 chamber containing an artificial cerebrospinal fluid (ACSF) composed of (in mM) 126
391 NaCl, 3.5 KCl, 1.2 NaH_2PO_4, 1.3 $MgCl_2$, 2 $CaCl_2$, 25 $NaHCO_3$, 10 D-glucose (pH = 7.3-
392 7.4) at RT for at least 1 h before recording. The two last solutions were saturated with
393 95% O_2 and 5% CO_2.

394 ***Whole-cell voltage-clamp recordings***

395 Slices were submerged in a low-volume recording chamber and continuously
396 superfused with 32-34°C ACSF at 5 ml/min perfusion rate. For each mouse, four slices
397 containing the dDG were selected for patch clamp recordings. DG neurons were
398 visualized by infrared video microscopy using an upright microscope (SliceScope,
399 Scentifica Ltd). Patch pipettes were pulled from borosilicate glass tubing (1.5 mm outer
400 diameter, 0.5 mm wall thickness) and filled with an intracellular solution containing (in
401 mM) 20 CsCl, 115 CsGlu, 10 HEPES, 1.1 EGTA, 4 MgATP, 10 Na phosphocreatine and
402 0.4 Na_2GTP as well as 0.2% biocytin for *post-hoc* morphological identification of the
403 recorded neuron (see below). The pipette resistance was 4–6 MΩ. Recordings were
404 performed in the Apex, upper and lower blades of the dDG. Signals were fed to a
405 Multiclamp 700A (Molecular Devices), digitized (10 kHz) with a DigiData 1550
406 (Molecular Devices) interface to a personal computer and analysed with ClampFit
407 software (Molecular Devices). Optical stimulation of ChR2-expressing axon terminals
408 was performed by pulses of 470 nm blue light delivered by a LED (pE-2, CoolLED)
409 through a 40X objective attached to microscope (SliceScope, Scientifika Ltd).
410 Stimulations consisted of paired 5 ms pulses (500 ms between pulses, every 30 s). For
411 VGLUT2-ChR2 mice, the light intensity corresponded to 20-30% (1.6-2.5 mW) of the
412 LED maximum power (7.5 mW) and for the VGLUT2-EYFP control mice, it varied

413 between 20 to 90% (6.9 mW) of LED maximum power. Postsynaptic current (PSC)
414 responses to optic stimulations were recorded at different holding potentials ranging
415 from -70 mV (close to reversal potential of GABA-A currents but far below the reversal
416 potential of glutamate receptor-mediated currents) to +10mV (close to reversal potential
417 of glutamate receptor-mediated currents but far above the reversal potential of GABA-A-
418 mediated currents). Pharmacological characterization of inhibitory PSCs (IPSCs) and
419 excitatory PSCs (EPSCs) was achieved using antagonists of GABA-A, AMPA and
420 NMDA receptors. We used Gabazine or bicuculline (antagonist of GABA-A receptors,
421 10 μM), D-AP5 (antagonist of NMDA receptors, 40 μM) and NBQX (antagonist of AMPA
422 and Kaïnate receptors, 10 μM). The co-release of glutamate and GABA was further
423 demonstrated in several DG granule cells (n=5), by recording first light stimulated PSC
424 at -70 mV (Figure 4K). At this holding potential the recorded currents were essentially
425 generated by glutamate receptors. Then the glutamate component was abolished by
426 NBQX and D-AP5, and the GABA component was revealed at +10 mV holding potential.
427 This PSC was completely inhibited by bicuculline application that confirmed the GABA
428 receptor origin of these remaining currents (see also Figure 4J).

429 ***Double immunohistofluorescent labeling for Biocytin and GFP***

430 After recordings slices were processed for simultaneous detection of the biocytin-filled
431 neurons and GFP-labeled axon fibers and terminals in order to identify the recorded
432 cells and evaluate the efficiency of the transfection, respectively. Slices were fixed
433 overnight at 4°C in a solution containing 4% PFA in PB. Then they were rinsed in PB,
434 cryoprotected in 20% sucrose and quickly frozen on dry ice. After several rinses in
435 KPBS, slices were incubated in a solution containing normal donkey serum (NDS, 1:30;
436 Vector Laboratory) diluted in KPBS with 0.3% Triton- X100, for 2 h at RT. They were

437 incubated in a solution containing goat anti-biotin (1:200) and rabbit anti-GFP (1:2000),
438 diluted in KPBS containing 0.3% Triton-X100 and NDS (1:100), overnight at RT. After
439 several rinses in KPBS, slices were incubated for 2 h in Alexa488-conjugated donkey
440 anti-goat IgG (1:200); Invitrogen), and Cy3-donkey anti-rabbit IgG (1:100) diluted in
441 KPBS with 0.3% Triton-X100. After rinses in KPBS, slices were mounted on slides and
442 coverslipped with Fluoromount. The specimens were analyzed with a fluorescence
443 microscope (Nikon 50i) or confocal microscope (Zeiss).
444
445 ***In vivo* electrophysiology: optic stimulation, LFP and EEG recordings**
446 All mice were placed for 7 days in a recording box in order to get them used to the
447 recording conditions. The recording box was ventilated, as well as electrically and sound
448 isolated. The temperature was regulated at 21°C, and a 12 h light/12 h dark cycle
449 imposed. Mice were accustomed to the cable connecting them to the recording device.
450 The recording cable connected the micro-connector implanted on the head of the animal
451 to a collector, which ensured the continuity of the recorded signals without hindering the
452 movements of the mouse. At the end of this habituation, the control recordings begun.
453 EEG and EMG recordings were digitized at 1 kHz, amplified 5000 times with a 16
454 channels amplifier (A-M System) and collected on a computer via a CED interface using
455 Spike 2 software (Cambridge Electronic Design). The signal was band-pass filtered
456 online between 1 and 300 Hz for EEG, and between 10 and 100 Hz for EMG. The 50 Hz
457 signal was removed with a notch filter. The EEG and LFP signals were acquired by
458 monopolar derivation (differential between the recording electrode and the reference
459 electrode located above the cerebellum). The EMG bipolar signals were calculated by

460 measuring the differential between the two EMG electrodes. Mice were recorded for 24
461 h of baseline followed by optogenetic manipulation.

462 ***In vivo optogenetic stimulation***

463 Optical stimulations were delivered via a patch cable connected to a 100 mW 473-diode
464 (Laserglow). Stimulations were performed during 4 days: in the first 3 days, mice were
465 stimulated during one specific vigilance state par day: waking (WK), slow wave sleep
466 (SWS) or PS. Each day, stimulations were delivered during the same circadian period
467 (10 AM–2 PM). Stimulations were applied 10 s after the occurrence of a stable WK,
468 SWS or PS event as detected by real time observation by the experimenter. For WK and
469 SWS, stimulations were spaced apart by at least 1 min and for PS, by at least 15 s.
470 Blue exciting stimulations consisted of 10-s trains of 10-ms pulses at 20 Hz. Light power
471 at the fiber tip was 10 mW.
472 The 4th day of experiments, 4 VGLUT2-EYFP and 4 VGLUT2-ChR2 animals were
473 stimulated for 15 min at 20 Hz (10-ms pulses). All mice were euthanized 90 min after the
474 beginning of the stimulation by transcardiac perfusion of 4% PFA. Brain tissues were
475 processed for immunohistochemical detection of cFos expression (see above).

476 ***Analysis of the sleep wake states***

477 Polysomnographic recordings were visually scored by 5 s epochs for WK, SWS and PS
478 as previously described (Sapin et al. 2009). Hypnograms were obtained by using a
479 custom Matlab script. For each animal, the number of awakenings during SWS and PS
480 optogenetic stimulations was counted and expressed as percentage of the total number
481 of stimulations.

482

483

484 ***LFP and EEG analysis***

485 LFP and EEG signals were analyzed using a custom Matlab script using the Chronux
486 toolbox. The time-frequency spectrograms were computed with the same toolbox and
487 expressed in arbitrary units. The mean power spectral density in the 10 s before the
488 stimulation was compared to that in the 10 s during the stimulation (sliding window: 1 s),
489 in order to obtain a mean spectral power ratio (PR) ± SEM. The frequency spectra were
490 grouped into frequency bands commonly used Delta: 1-4 Hz, Theta: 6-12 Hz, Sigma: 12-
491 14 Hz, Beta: 15-30 Hz, Gamma: 30-100 Hz. Power spectral values at 20 Hz and its
492 harmonics were excluded from the analysis.

493 To analyze the evolution of LFP and EEG theta and gamma bands during optogenetic
494 stimulation, the mean PR of these spectral bands and the respective 95% confidence
495 intervals were calculated from 10 s before to 10 s after the photostimulation. In order to
496 compute these intervals, we used a bootstrap procedure, which allows creating artificial
497 groups from the original data, with replacement. The mean of each artificial group
498 derived from the original data was then computed. This operation was repeated 10000
499 times and the 95% confidence interval was the 5th and the 95th percentile of the means
500 of the randomly constructed samples.

501 Finally, during WK and PS the peak of theta frequency (6-12 Hz) in the 10 s before and
502 during the optogenetic stimulation was identified in all animals.

503 Analysis of variance (Mann-Whitney test) was performed on the percentage of
504 awakenings, the mean spectral power ratios and the theta frequency peaks. These
505 statistics were performed using Statview software (StatView Inc, Nestbit, NS).

506

507

508 ***EMG analysis***

509 EMG signals during WK were analyzed using a custom Matlab script. The mean EMG
510 value in the 10 s before the stimulation was compared to that in the 10 s during the
511 stimulation, in order to obtain a mean EMG ratio ± SEM. In the 2 groups of animals we
512 performed a sequential analysis per 0.5 s on the mean of the absolute EMG values from
513 20 seconds before to 10 seconds after the photostimulation. The respective bootstrap
514 95% interval (computed as described above) was calculated for each sequential value.
515 Further, analysis of variance (Mann-Whitney test) was performed on the EMG mean by
516 using Statview software.

517

518

518 ## Results

519 **Distribution of VGAT and/or VGLUT2 mRNA-containing neurons in the SuM of**
520 **VGLUT2-Cre transgenic mice**

521 Three populations of VGAT and/or VGLUT2 mRNA-containing neurons were observed
522 at all antero-posterior levels of the SuM. These included a population of large neurons
523 co-expressing VGAT and VGLUT2 mRNA (Figure 1 A, D, arrows); and two populations
524 of smaller neurons containing either VGAT mRNA (Figure 1 A, D, arrowheads) or
525 VGLUT2 mRNA (Figure 1 A, D, blue). The distribution as well as the density of these
526 populations differed significantly within the SuM. Almost all VGAT/VGLUT2 mRNAs –
527 containing neurons were clustered around and above the mammillary tract (mt) (Figure 1
528 A, D) in a region similar to that described in rats as the grandicellular SuM (SuMg) by
529 Pan and Mc Naughton (2004) and that is included in the lateral SuM (SuML) region of
530 Paxinos and Franklin's mouse Atlas. The numerous singly labeled VGLUT2 mRNA -
531 expressing cells were small and mostly located in the most central area (Figure 1 A)
532 termed the parvicellular SuM (SuMp) by Pan & Mc Naughton (2004) corresponding to
533 the SuMm in Paxinos and Franklin's mouse Atlas. Some were also intermingled with the
534 larger VGAT/VGLUT2 mRNAs-containing cells in the SuMg. Few neurons expressed
535 VGAT mRNA only. These neurons were scattered within the SuML and SuMM.

536 In summary, our results indicate that in mice like in rats a large number of neurons co-
537 expressing markers of GABAergic and glutamatergic transmission are located in the
538 SuML region.

539

540

541 **Distribution of SuM neurons with dorsal dentate gyrus (dDG) projections**

542 Unilateral or bilateral injections of rabies-virus (RV) were performed into the DG of the
543 dorsal hippocampal formation (Figure 1 B, insert) to evaluate the distribution and
544 proportion of SuM neurons that project to this structure. In all these mice, the RV tracer
545 injection was located either in the granule cell layer or inner molecular region of the
546 dorsal blade of the DG. Within the SuM, all these animals displayed retrogradely labeled
547 neurons exclusively in the region of SuML (SuMg) immediately dorsal to the mt (Figure 1
548 B, E, H). Virtually none were found in the SuMM (Figure 1 B). Many of these neurons
549 displayed a large soma with several labeled proximal dendrites (Figure 1 E). Therefore
550 in mice, SuM neurons innervating the dDG are located in the SuML as in rats (Soussi et
551 al., 2010).

552

553 **Neurotransmitter phenotype of SuM neurons projecting to the dDG revealed by**
554 **simultaneous detection of RV retrograde tracer, VGAT mRNA, and VGLUT2 mRNA**

555 We next investigated whether the SuML neurons projecting to the dDG express markers
556 of GABAergic and glutamatergic transmissions. Sections processed for simultaneous
557 detection of VGAT mRNA, VGLUT2 mRNA and RV (Figure 1 A-I) showed that almost all
558 RV retrogradely-labeled neurons co-express VGAT and VGLUT2 mRNAs (Figure 1 A-I,
559 arrows). These data were confirmed by quantitative analysis performed on twelve
560 sections (4 mice; 3 sections per mouse) showing that 99% (n= 378 out of 380 neurons)
561 of the RV-labeled neurons co-expressed VGAT and VGLUT2 mRNAs. The percentages
562 of these triple-labeled cells were the same (99%) for the three antero-posterior levels of
563 the SuM analyzed (range 98%-100%).

564

565 **Distribution and neurotransmitter phenotype of fibers and axon terminals**
566 **originating from SuM neurons innervating the dorsal dentate gyrus**

567 To further characterize the neurochemical properties of SuML neurons innervating the
568 dDG, AAV-5-DIO-EYFP was injected bilaterally in the SuML (Figure 2 A) allowing
569 specific EYFP labeling of VGLUT2 neurons and of their axon fibers innervating the
570 hippocampus including the dDG (Figure 2 A). Sections of these VGLUT2-EYFP mice
571 were processed for simultaneous immunohistofluorescent detection of EYFP, VGLUT2
572 and VGAT or GAD65. All mice injected in the SuML displayed numerous anterograde–
573 EYFP labeled fibers and axon terminals in the dDG (Figure 2 B, arrowheads) on both
574 sides of the hippocampal formation. Labeled fibers and axon terminals were also
575 present in the CA2/CA3a region of the hippocampus in particular when the injection
576 sites involved more posterior levels of the SuML (Figure 2 B, arrowheads).

577 In the dDG, EYFP axonal fibers and terminals were mainly located in the supragranular
578 layer of the dorsal and ventral blades of the DG (Figure 2 B-D) although some were
579 localized in the granule cell layers. In all triple labeled sections either for EYFP, GAD65
580 and VGLUT2 or EYFP, VGAT and VGLUT2, the vast majority if not all EYFP-containing
581 axon terminals present in the supragranular and granule cell layers were labeled for both
582 GAD65 and VGLUT2 (Figure 2 C, E-H) or VGAT and VGLUT2 (Figure 2 D, I-L).
583 Quantitative analysis of double labeling for VGLUT2 and VGAT showed that 90% (range
584 82% to 99%) of VGLUT2 labeled terminals were labeled for VGAT with no major
585 differences between the infragranular blade (89%; range 82% to 99%) and the
586 supragranular blade (91%; range 83% to 99%). Further quantification of EYFP labeling
587 revealed that 98 % (range 96% and 100%) of the axon terminals contained both VGAT
588 and VGLUT2 confirming that all EYFP-containing axon terminals originating from SuML

589 neurons contained both markers of GABA and glutamate neurotransmissions.

590

591 **Electron microscopy analysis of synaptic contacts established by EYFP-**
592 **containing axon terminals originating from SuML neurons**

593 In the supragranular region of the dDG, axon terminals from SuML neurons labeled for
594 EYFP displayed diffuse electron-dense labeling that contrasted with adjacent unlabeled
595 cellular compartments. These labeled axon terminals formed synaptic contacts on the
596 soma (Figure 3 A, B, D, E, F, I) and dendritic profiles (Figure 3 C, G, H) of presumed
597 granule cells (GCs). These axon terminals were often very large boutons that displayed
598 one (Figure 3 A, B, D, E) or more (Figure 3 F) synaptic zones with relatively thin post-
599 synaptic densities (arrowheads) characteristic of symmetric synapses. Other synaptic
600 contacts formed by these labeled terminals displayed thicker post-synaptic densities
601 characteristic of asymmetric synapses (Figure 3 A, B, C; arrow). We also observed large
602 labeled "en passant" boutons establishing symmetric synapses on the dendrites of a
603 presumed granule cell (Figure 3 G, H). Finally, some axon terminals from SuML neurons
604 formed both symmetric (arrowhead) and asymmetric (arrow) synapses on the soma or
605 the proximal dendrite of two different neighboring GCs (Figure 3, A, B).

606 Together these data demonstrate that in mice all SuM neurons innervating the dDG
607 belong to a single population of large neurons located in the SuMg region of the SuML.
608 These cells display a dual neurochemical phenotype for GABA and glutamate
609 neurotransmissions and establish symmetric (presumably inhibitory) and asymmetric
610 (presumably excitatory) synapses on the GCs of the dDG.

611

612

613 **Co-release of glutamate and GABA at the SuML-dentate granule cells synapses**

614 The neurochemical profile of SuML neurons projecting to the dDG strongly suggested
615 that they co-release GABA and glutamate at the SuML-dentate granule cells synapses.
616 To test this hypothesis, we performed patch clamp recordings of dDG granule cells layer
617 using optogenetic stimulation in hippocampal slices obtained from VGLUT2-ChR2 mice
618 (5 mice, 3 sections per mouse, 16 neurons) and VGLUT2-EYFP control mice (3 mice, 3
619 sections per mouse, 10 neurons) (Figure 4). The light stimulation of SuML-DG fibers and
620 axonal terminals expressing ChR2 (Figure 4 A) evoked a fast inward and a slower
621 outward synaptic current in fourteen out of sixteen neurons recorded at a holding
622 potential of -30 mV (Figure 4 D, F, H). Post-hoc immunodetection of biocytin-filled
623 neurons showed that all these recorded neurons correspond to GCs (Figure 4 C, E, G,
624 I). They were equally distributed in the apex and the upper and lower blades of dDG
625 granule cell layer (Figure 4 B). These GCs were additionally recorded at different holding
626 potentials. At -10 mV and +10 mV (close to the reversal potential of the glutamatergic
627 receptor-mediated currents), only the outward (positive going) synaptic current was
628 observed (Figure 4 D, see also F, H). From -70 mV to -50mV (close to the reversal
629 potential of GABA-A receptor-mediated currents) only the inward (negative going)
630 synaptic current was observed (Figure 4 D, see also 4 F, 4 H). At intermediate holdings,
631 from -30 to -20mV, the light-evoked synaptic currents displayed both inward and
632 outward components (Figure 4 D, F, H). Using a pharmacological approach, we
633 confirmed the nature of these currents. Bath application of a mixture of AMPA/Kainate
634 and NMDA receptor antagonists (NBQX 10 μM and D-AP5 40 μM) abolished the inward
635 component (Figure 4 F, K, L, red trace) while GABA-A receptor blockers inhibited the
636 outward component (Figure 4 H, J- gabazine; K, L– bicuculline, green trace).

637 Quantitative analysis performed in 5 DG neurons (Fig. 4 K) further illustrated that in
638 regular ACSF the repetitive light pulses (5 ms, 0.05 Hz) evoked postsynaptic currents
639 (PSC) of relatively stable amplitude (1.00 ± 0.26 normalized, Fig. 4 K, L, left hand side
640 red trace is an example of an averaged response of one neuron). The application of
641 glutamate receptor blockers (10 μM NBQX + 40 μM D-AP5) reduced the peak amplitude
642 by 84% (0.16 ± 0.15, $p<0.01$, n= 5, paired Wilcoxon test). The remaining response seen
643 in 4 out of 5 neurons was probably due to GABA-A mediated current because at -70 mV
644 the driving force for chloride driven currents is close to but is not zero (Figure 4 K, L, red
645 trance in the middle). Therefore in case of GABA massive release some inward current
646 is still possible. Indeed a switch to Vh= 10 mV revealed a large PSC response to light
647 stimulation (Figure 4 L, green trace in the middle) which had a stable amplitude (1.00 ±
648 0.20 normalized), and was subsquently reduced to 12% (0.12 ± 0.16, $p<0.01$, n= 5,
649 paired Wilcoxon test) by the addition of 10 μM bicuculline to the ACSF already
650 containing GluR blockers (Figure 4 L, green trace at left). In 3 out of 5 neurons,
651 bicuculline completely abolished the synaptic response to light pulses after 6 min of drug
652 perfusion. In two neurons the small remaining current was probably due to the fact that
653 bicuculline is a competitive antagonist and can be displaced when large quantities of
654 GABA are released. All these results indicate that the inward synaptic current
655 component is mediated by glutamate and the outward component by GABA.
656 Importantly, the disappearance of the inward (glutamatergic) component induced by the
657 light stimulation in the presence of NBQX and D-AP5 antagonists (red trace) did not
658 affect the outgoing (GABAergic) currents (Fig. 4 F). In two GCs (Figure 4 I), the
659 disappearance of the glutamate response (incoming current recorded at -30 mV) in the

660 presence of NBQX and AP5 (red trace) unmasked the GABAergic component (outgoing
661 current) abolished after addition of gabazine (green trace) (Figure 4 J).
662 The very short latency of the glutamatergic inward and GABAergic outward currents
663 recorded in a GC after light stimulation of ChR2 containing axon terminals, and the
664 persistence of GABAergic outflow current in the presence of NBQX and AP5 indicates
665 that the GABAergic current results from direct light stimulated GABA release and not
666 from the excitation of DG GABAergic neurons by light stimulated glutamate release.
667 Together, these results suggest that activation of SuML axon terminals produce
668 monosynaptic glutamatergic and GABAergic currents on their targets.
669 Finally, we verified that light stimulation (5 ms, 10%, 50% 90% max power LED) of fibers
670 and axon terminals expressing EYFP on slices of control VGLUT2-EYFP mice (n= 3) did
671 not evoke any response in the recorded GCs (n= 10) (Figure 4 M, N).
672
673 **Effect of optogenetic stimulation of SuML axon terminals innervating the dDG on**
674 **behavior, LFP and EEG spectral content**
675 We analysed the effects of light stimulation of SuML axon terminals innervating the dDG
676 on behavioral states, spectral content of the LFP recorded in dDG and cortical EEG in
677 VGLUT2-ChR2 (n= 4) and control VGLUT2-EYFP mice (n= 4).
678 Light activation of SuML axon terminals in VGLUT2-ChR2 mice during waking (WK),
679 induced a strong and significant increase in EMG value as compared to control mice
680 (mean EMG ratio, VGLUT2-EYFP= 0.9 ± 0.03, VGLUT2-ChR2= 2.0 ± 0.31, p= 0.0209).
681 The increase in EMG was due to an increase in animal movements (Figure 5 A, D). It
682 was associated with a slight but not significant increase in theta power in the dDG LFP
683 (Figures 5 B; 6 A) and the EEG (Figure 7 A) compared to control VGLUT2-EYFP mice.

684 However, theta/delta ratio was significantly increased both in the dDG LFP (Figure 6 A,
685 B) and the EEG (Figure 7 C, D) during the stimulation compared to control mice (LFP:
686 VGLUT2-ChR2= 1.3 ± 0.11, VGLUT2-EYFP= 0.9 ± 0.02, p=0.0209, EEG: VGLUT2-
687 ChR2= 2.2 ± 0.31, VGLUT2-EYFP= 0.9 ± 0.05, p=0.0209). The frequency at the theta
688 peak was slightly but not significantly increased during stimulation as compared to
689 control VGLUT2-EYFP animals (LFP: VGLUT2-ChR2: 8.43 ± 0.43 Hz, VGLUT2-EYFP:
690 6.96 ± 0.23 Hz, p= 0.0833) (Figures 5 B; 6 D). Gamma power (30-100 Hz) was
691 significantly increased during the stimulation in VGLUT2-ChR2 mice as compared to
692 control mice in the dDG LFP (VGLUT2-ChR2= 1.6 ± 0.13, VGLUT2-EYFP= 1.0 ± 0.02,
693 p=0.0209) (Figures 5 C; 6 A, C) and in the EEG (VGLUT2-ChR2: 1.68 ± 0.05, VGLUT2-
694 EYFP: 0.98 ± 0.02, p=0.0209 (Figure 7 B, C, E). The increase occurred immediately
695 after the beginning of the stimulation and lasted until the end of it (Figures 6 C; 7 E).
696 Stimulations during SWS induced significantly more often an awakening in VGLUT2-
697 ChR2 than in control VGLUT2-EYFP mice (p=0.0209, VGLUT2-ChR2: 80 % of the
698 cases, range 40%-100%; VGLUT2-EYFP: 15 % of the cases, range: 0%-30%; Figure 5
699 E, H). The induced waking state lasted at least the duration of the stimulation and was
700 characterized by a significant increase in theta/delta ratio (LFP: VGLUT2-ChR2= 1.3 ±
701 0.14, VGLUT2-EYFP= 1.0 ± 0.02, p=0.0433; EEG: VGLUT2-ChR2= 1.5 ± 0.27,
702 VGLUT2-EYFP= 1.0 ± 0.03, p=0.0209) (Figures 6 A, B; 7 C, D) and a decrease of delta
703 power both in the dDG LFP (VGLUT2-ChR2= 0.6 ± 0.11, VGLUT2-EYFP= 0.9 ± 0.01,
704 p=0.0209) and the EEG (VGLUT2-ChR2= 0.5 ± 0.13, VGLUT2-EYFP= 0.9 ± 0.02,
705 p=0.0209) in VGLUT2-ChR2 compared to control VGLUT2-EYFP mice (Figures 5 E, F;
706 6 A; 7 A, C). This induced waking state was also associated with an increase in gamma

707 power in the dDG LFP (Figures 5 E, G; 6 A, C) and in the EEG (VGLUT2-ChR2= 1.36 ±
708 0.16, VGLUT2-EYFP 0.99 ± 0.03, p=0.0433) (Figure 7 B, C, E).
709 In contrast to SWS, light stimulation of SuML axon terminals in the dDG of VGLUT2-
710 ChR2 mice during PS did not induce significantly more awakening in VGLUT2-ChR2
711 mice compared to control VGLUT2-EYFP animals (p= 0.3865; Figure 5 L).
712 Light activation of SuML axon terminals during PS in VGLUT2-ChR2 induced a
713 significant increase in theta power compared to VGLUT2-EYFP mice in the dDG LFP
714 (Figures 5 I, J; 6 A, B; VGLUT2-ChR2= 1.3 ± 0.04, VGLUT2-EYFP= 0.9 ± 0.02, p=
715 0.209) but not in the EEG (Figure 7 C, D; p= 0.773). The frequency at the theta peak
716 was also significantly increased in the dDG LFP compared to control EYFP-VGLUT2
717 animals (VGLUT2-ChR2: 8.3 ± 0.13 Hz, VGLUT2-EYFP: 7.7 ± 0.15 Hz, p= 0.0209)
718 (Figure 6 E). In addition, gamma was significantly increased both in the dDG LFP and
719 the EEG during the stimulation in VGLUT2-ChR2 mice compared to control VGLUT2-
720 EYFP mice (LFP: VGLUT2-ChR2= 1.1 ± 0.02, VGLUT2-EYFP= 1.0 ± 0.01, p= 0.0209;
721 EEG: VGLUT2-ChR2: 1.68 ± 0.05, VGLUT2-EYFP: 0.98 ± 0.02, p= 0.0209; Figures 5 K,
722 6 A, C; 7 B, C, E).
723
724 **Effect of optogenetic activation of SumL axon terminals innervating dDG on**
725 **cFos expression**
726 Mouse brains were processed for immunohistochemical detection of cFos in order to
727 assess the effect of SuML axon terminal activation on DG cell activity. Whereas only a
728 few neurons were labeled for cFos in the GCL of the DG in control VGLUT2-EYFP mice
729 (n= 4) (Figure 8 A, B), numerous neurons strongly labeled for cFos were observed in the
730 granule cell layer of the dDG in VGLUT2-ChR2 mice (n= 4) (Figure 8 C, D). Quantitative

731 analysis showed a 241% increase in the number of labeled cFos neurons in the dDG
732 ipsilateral to the stimulation site (270 ± 33) as compared to control mice (ipsi: 79 ± 23;
733 p= 0.026; Figure 8 E) whereas no significant difference was observed in the
734 contralateral dDG (VGLUT2-ChR2: 178 ± 21; VGLUT2-EYFP contra: 90 ± 33; p=0.2;
735 Figure 8 E).
736

736 ## Discussion

737 **Neuroanatomical and "in vitro" experiments showing the dual glutamate-GABA**
738 **feature of the SuML-DG pathway**

739 Our results first establish at the neuroanatomical level that in mice as in rats (Soussi et
740 al., 2010), all SuM neurons innervating the dDG display a dual GABAergic and
741 glutamatergic neurotransmitter phenotype. We further demonstrate that these neurons
742 correspond to a population of SuM cells located just dorsal to the mammillary tract that
743 likely correspond to grandicellular neurons described in rat within the SuML region
744 (Paxinos and Watson 1998) or SuMg (Pan and McNaughton 2004). In addition, our EM
745 data show that SuML terminals form asymmetric (presumed excitatory glutamate)
746 synapses onto some GCs and symmetric (presumed inhibitory GABA) synapses onto
747 others as previously described in rat (Boulland et al., 2009; Soussi et al., 2010). We
748 further found in this study that one axon bouton from a SuML neuron can form an
749 asymmetric synapse on a GC and a symmetric synapse on another GC. In agreement
750 with these neuroanatomical results, our *in vitro* electrophysiological experiments show
751 that optical stimulation of SuM axon terminals innervating the dDG induce co-release of
752 GABA and glutamate on almost all dentate GCs in line with two recent studies
753 (Pedersen et al 2017; Hashimotodani et al., 2018). Hashimotodani et al. (2018) further
754 showed that such co-transmission of GABA and glutamate induce net excitatory effects
755 on GCs and potentiate GC firing when temporally associated with perforant path inputs.
756 In line with such hypothesis, after *in vivo* optic stimulation of SuML axon terminals
757 innervating the dDG in VGLUT2-ChR2 mice, we found that a significant number but not
758 all GCs neurons below the optic fiber were labeled with cFos. Therefore, these cFos

759 labeled neurons could constitute a population of GCs that are simultaneously activated
760 by the optic stimulation of SuML axon terminals and perforant path inputs.
761
762 **Effect of optogenetic stimulation of SuML-DG fibers on vigilance states**
763 Activation of SuML axon terminals projecting to the DG induces an awakening effect in
764 mice when performed during SWS but not during PS. It has been shown by Renouard et
765 al. (2015) that the SuML-DG pathway is active during PS and therefore its stimulation
766 during this state might not induce WK because the pathway is already engaged and its
767 overactivation might therefore not to be sufficient to awaken the animal. In contrast,
768 when the stimulation occurs during SWS, an awakening is induced likely because the
769 path is normally inactive during this state. It can be proposed that the stimulation of the
770 DG granule cells by the SuML induces the reactivation of memories and subsequently of
771 structures involved in the exploration leading to an awakening of the animal during
772 SWS. It might also be due to the fact that there is no muscle atonia during this state
773 compared to PS. In line with such hypothesis, stimulation during WK induces increased
774 motor and exploratory activity. Such result is in line with the literature since an increase
775 in exploratory activity was reported when stimulating with blue light dDG neurons
776 expressing ChR2 (Kheirbek et al., 2013).
777
778 **Optogenetic stimulation of SuML-DG fibers increases gamma and theta**
779 Our study further demonstrates that activation of SuML axon terminals innervating the
780 DG during PS increases theta power and frequency as well as gamma power in the DG
781 LFP and to a minor extent in the EEG. Activation of the SuML fibers during WK also
782 induces an increase of gamma power in the DG LFP and EEG associated with an

783 increased locomotion. During SWS, the activation of the SuML-dDG pathway induced
784 awakening and a switch from delta to theta activity and an increase in gamma power
785 both in DG LFP and EEG.
786 It has been previously shown that the SuM can exert significant modulatory control of
787 the theta rhythm (Vertes and Kocsis, 1997). A large percentage of SuM neurons
788 discharge rhythmically, in phase with theta (Kirk and McNaughton, 1991, Kocsis and
789 Vertes, 1994) and this activity is independent of that occurring in the hippocampus.
790 Indeed, neurons in the SuM continue to fire bursts in the theta range frequency after
791 lesion or pharmacological inactivation of the medial septum (Kirk and McNaughton,
792 1991) known to abolish theta rhythmic activity in the hippocampus. Further, electrical
793 stimulation or carbachol injections in the SuM synchronously drive theta phase-locked
794 cells in both septum (Bland et al., 1994) and hippocampus (Colom et al., 1987). In
795 addition, the SuM controls the frequency and amplitude of theta (Kirk and McNaughton,
796 1993). These results indicated that the SuM plays a role in theta occurrence but
797 experiments were performed in anesthetized animals and did not specifically study the
798 SuML-DG pathway like in the present study. Indeed, SuM neurons also project directly
799 to the medial septum (Vertes and McKenna, 2000) and can influence theta through the
800 latter structure as well.
801 Our results also show that the frequency at the peak of theta is higher during PS than in
802 WK in basal conditions. Further, we found out that optical stimulation of SuML-DG fibers
803 during PS induced a similar increase of the frequency at the peak of theta. Besides,
804 lesion of the SuM induced a decreased of theta power specifically during PS (Renouard
805 et al., 2015). On the other hand, lesion of all neurons or specific inactivation of the
806 GABAergic neurons of the medial septum strongly decreases theta during PS and WK

807 (Mitchell et al., 1982, Green and Arduini, 1954, Boyce et al., 2016). Our data also show
808 that stimulation of the SuML-DG fibers induces an increase in gamma power in the dDG
809 and also in the EEG both during PS and WK. Interestingly, Montgomery et al. (2008)
810 found by coherence analysis that dentate/CA3 theta and gamma power and synchrony
811 were significantly higher during PS compared with active WK and that, in contrast,
812 gamma power in CA1 and CA3-CA1 gamma coherence showed significant decreases
813 during PS. These and our results strongly suggest that the medial septum GABAergic
814 neurons induces theta both during WK and PS whereas the increase of theta and
815 gamma power and theta frequency occurring in the DG during PS compared to WK is
816 induced by the projection from the SumL.
817
818 **Functional role of the SumL-DG pathway**
819 It has been previously shown that GCs of the DG are instrumental for spatial
820 discrimination (McHugh et al., 2007). In particular, it has been shown that small
821 populations of GCs (2-4%) representing memory engrams are specifically activated
822 when the animals are exposed to a specific context. These cells are reactivated each
823 time the animal is re-exposed to the same context (Schmidt et al., 2012). Optogenetic
824 activation in a different context of a DG engram activated during contextual fear
825 conditioning induces freezing (Liu et al., 2012). Conversely, inactivation during
826 contextual fear memory recall of the DG GCs activated during encoding decreases
827 freezing (Denny et al., 2014). These results indicate that activation of memory engrams
828 composed of DG GCs cells is necessary for spatial learning. Interestingly, in these
829 studies, the mean number of neurons labeled with cFos or Arc in one section (35 μm) of
830 the DG after contextual fear conditioning was in the 30-60 range. In the present study,

during stimulation of the SuML fibers in the DG, a mean of 67 DG cells were expressing cFos in the DG per section (40 µm). Finally, Renouard et al. (2015) counted a mean of 68 Arc- and 66 cFos- labeled neurons in one DG section after PS hypersomnia in rats. Therefore, approximatively the same number of DG GCs cells is activated during encoding of a contextual fear memory, stimulation of the SuML fibers in the DG and PS hypersomnia. First, the fact that a similar number of cells are activated when stimulating SuML terminals as during PS hypersomnia suggests that the activation seen during PS is likely due to activation of the SuML-DG pathway. Second, the fact that a similar number of cells are activated during a memory task as during PS hypersomnia and stimulation of the SuML fibers suggest that memory engrams could be activated in these two conditions. Therefore, the induction of an active behavior when the stimulation is made during WK could be due to the activation of memory engrams. Since only a limited number of GCs cells are activated during PS and SuML terminals stimulation despite the fact that a large number of GCs neurons seems to be innervated by SuML axon terminals, it also suggests that activation of these cells is due to a conjunction of the SuML input with another excitatory input. It can be proposed that the medial entorhinal input is involved since it is the main excitatory afferent to the DG involved in its activation during memory encoding (Sasaki et al., 2015). Such hypothesis remains to be tested using optogenetic manipulation of the activated neurons during PS.

851 **References**

852 Billwiller F, Renouard L, Clement O, Fort P, Luppi PH (2017) Differential origin of the
853 activation of dorsal and ventral dentate gyrus granule cells during paradoxical (REM)
854 sleep in the rat. Brain Struct Funct 222:1495-1507.

855 Bland BH, Oddie SD, Colom LV, Vertes RP (1994) Extrinsic modulation of medial septal
856 cell discharges by the ascending brainstem hippocampal synchronizing pathway.
857 Hippocampus 4:649-60.

858 Bolte S, Cordelières FP (2006) A guided tour into subcellular colocalization analysis in
859 light microscopy. J Microsc 224:213-232.

860 Borhegyi Z, Leranth C (1997) Distinct substance P- and calretinin-containing projections
861 from the supramammillary area to the hippocampus in rats; a species difference
862 between rats and monkeys. Exp Brain Res 115:369-374.

863 Boulland JL, Jenstad M, Boekel AJ, Wouterlood FG, Edwards RH, Storm-Mathisen J,
864 Chaudhry FA (2009) Vesicular Glutamate and GABA Transporters Sort to Distinct Sets
865 of Vesicles in a Population of Presynaptic Terminals. Cereb Cortex 19:241-248.

866 Boyce R, Glasgow SD, Williams S, Adamantidis A (2016) Causal evidence for the role of
867 REM sleep theta rhythm in contextual memory consolidation. Science 352:812-816.

868 Bras H, Gaytán SP, Portalier P, Zanella S, Pásaro R, Coulon P, Hilaire G (2008)
869 Prenatal activation of 5-HT 2A receptor induces expression of 5-HT 1B receptor in
870 phrenic motoneurons and alters the organization of their premotor network in newborn
871 mice. Eur J Neurosci 28:1097-1107.

872 Colom LV, Ford RD, Bland BH (1987) Hippocampal formation neurons code the level of
873 activation of the cholinergic septohippocampal pathway. Brain Res 410:12-20.

874 Coulon P, Bras H, Vinay L (2011) Characterization of last-order premotor interneurons
875 by transneuronal tracing with rabies virus in the neonatal mouse spinal cord. J Comp
876 Neurol 519:3470-3487.

877 Denny CA, Kheirbek MA, Alba EL, Tanaka KF, Brachman RA, Laughman KB, Tomm
878 NK, Turi GF, Losonczy A, Hen R (2014) Hippocampal memory traces are differentially
879 modulated by experience, time, and adult neurogenesis. Neuron 83: 189-201.

880 Gonzalo-Ruiz A, Alonso A, Sanz JM, Llinás RR (1992) Afferent projections to the
881 mammillary complex of the rat, with special reference to those from surrounding
882 hypothalamic regions. J Comp Neurol 321:277-299.

883 Green JD, Arduini AA (1954) Hippocampal electrical activity in arousal. J Neurophysiol
884 17:533-57.

885 Haglund L, Swanson LW, Köhler C (1984) The projection of the supramammillary
886 nucleus to the hippocampal formation: An immunohistochemical and anterograde
887 transport study with the lectin PHA-L in the rat. J Comp Neurol 229:171-185.

888 Hashimotodani Y, Karube F, Yanagawa Y, Fujiyama F, Kano M (2018)
889 Supramammillary Nucleus Afferents to the Dentate Gyrus Co-release Glutamate and
890 GABA and Potentiate Granule Cell Output. Cell Rep 25:2704-2715

891 Kheirbek MA, Drew LJ, Burghardt NS, Costantini DO, Tannenholz L, Ahmari SE, Zeng
892 H, Fenton AA, Hen R (2013) Differential control of learning and anxiety along the
893 dorsoventral axis of the dentate gyrus. Neuron 77:955-968.

894 Kirk IJ, McNaughton N (1991) Supramammillary cell firing and hippocampal rhythmical
895 slow activity. Neuroreport 2:723-5.

896 Kirk IJ, McNaughton N (1993) Mapping the differential effects of procaine on frequency
897 and amplitude of reticularly elicited hippocampal rhythmical slow activity. Hippocampus
898 3:517-25.

899 Kocsis B, Kaminski M (2006) Dynamic changes in the direction of the theta rhythmic
900 drive between supramammillary nucleus and the septohippocampal system.
901 Hippocampus 16:531-540.

902 Kocsis B, Vertes RP (1994) Characterization of neurons of the supramammillary nucleus
903 and mammillary body that discharge rhythmically with the hippocampal theta rhythm in
904 the rat. J Neurosci 14:7040-7052.

905 Kocsis K, Kiss J, Csáki A, Halász B (2003) Location of putative glutamatergic neurons
906 projecting to the medial preoptic area of the rat hypothalamus. Brain Res Bull 61:459-
907 468.

908 Leranth C, Kiss J (1996) A population of supramammillary area calretinin neurons
909 terminating on medial septal area cholinergic and lateral septal area calbindin-containing
910 cells are aspartate/glutamatergic. J Neurosci 16:7699-7710.

911 Liu X, Ramirez S, Pang PT, Puryear CB, Govindarajan A, Deisseroth K, Tonegawa S
912 (2012) Optogenetic stimulation of a hippocampal engram activates fear memory recall.
913 Nature 484:381-385.

914 Maglóczky Z, Acsády L, Freund TF (1994) Principal cells are the postsynaptic targets of
915 supramammillary afferents in the hippocampus of the rat. Hippocampus 4:322-334.

916 Maquet P, Laureys S, Peigneux P, Fuchs S, Petiau C, Phillips C, Aerts J, Del Fiore G,
917 Degueldre C, Meulemans T, Luxen A, Franck G, Van Der Linden M, Smith C,
918 Cleeremans A (2000) Experience-dependent changes in cerebral activation during
919 human REM sleep. Nat Neurosci 3:831-836.

920 McHugh TJ, Jones MW, Quinn JJ, Balthasar N, Coppari R, Elmquist JK, Lowell BB,
921 Fanselow MS, Wilson MA, Tonegawa S (2007) Dentate gyrus NMDA receptors mediate
922 rapid pattern separation in the hippocampal network. Science 317:94-99.

923 Mitchell SJ, Rawlins JN, Steward O, Olton DS.(1982) Medial septal area lesions disrupt
924 theta rhythm and cholinergic staining in medial entorhinal cortex and produce impaired
925 radial arm maze behavior in rats. J Neurosci 2:292-302

926 Montgomery SM, Sirota A, Buzsáki G (2008) Theta and gamma coordination of
927 hippocampal networks during waking and rapid eye movement sleep. J Neurosci
928 28:6731-41.

929 Nitsch R, Leranth C (1996) GABAergic neurons in the rat dentate gyrus are innervated
930 by subcortical calretinin-containing afferents. J Comp Neurol 364:425-438.

931 Pan WX, McNaughton N (2002) The role of the medial supramammillary nucleus in the
932 control of hippocampal theta activity and behaviour in rats. Eur J Neurosci 16:1797-
933 1809.

934 Pan WX, McNaughton N (2004) The supramammillary area: its organization, functions
935 and relationship to the hippocampus. Prog Neurobiol 74:127-166.

936 Pasquier DA, Reinoso-Suarez F (1976) Direct projections from hypothalamus to
937 hippocampus in the rat demonstrated by retrograde transport of horseradish peroxidase.
938 Brain Res 108:165-169.

939 Pasquier DA, Reinoso-Suarez F (1978) The topographic organization of hypothalamic
940 and brain stem projections to the hippocampus. Brain Res Bull 3:373-389.

941 Paxinos G, Franklin KB (2005) The Mouse Brain in Stereotaxic Coordinates - 5th
942 Edition. Academic Press, San Diego.

943 Paxinos G, Watson, C (1998) The Rat Brain in Stereotaxic Coordinates, Academic
944 Press, Sydney.

945 Pedersen NP, Ferrari L, Venner A, Wang JL, Abbott SBG, Vujovic N, Arrigoni E, Saper
946 CB, Fuller PM (2017) Supramammillary glutamate neurons are a key node of the
947 arousal system. Nat Commun 8:1405.

948 Persson S, Boulland JL, Aspling M, Larsson M, Fremeau RT Jr, Edwards RH, Storm-
949 Mathisen J, Chaudhry FA, Broman J (2006) Distribution of vesicular glutamate
950 transporters 1 and 2 in the rat spinal cord, with a note on the spinocervical tract. J Comp
951 Neurol 497:683-701.

952 Raux H, Iseni F, Lafay F, Blondel D (1997) Mapping of monoclonal antibody epitopes of
953 the rabies virus P protein. J Gen Virol 78:119-124.

954 Renouard L, Billwiller F, Ogawa K, Clément O, Camargo N, Abdelkarim M, Gay N,
955 Scoté-Blachon C, Touré R, Libourel PA, Ravassard P, Salvert D, Peyron C, Claustrat B,
956 Léger L, Salin P, Malleret G, Fort P, Luppi PH (2015) The supramammillary nucleus and
957 the claustrum activate the cortex during REM sleep Sci Adv 1: *e1400177*.

958 Richmond MA, Yee BK, Pouzet B, Veenman L, Rawlins JN, Feldon J, Bannerman DM
959 (1999) Dissociating context and space within the hippocampus: effects of complete,
960 dorsal, and ventral excitotoxic hippocampal lesions on conditioned freezing and spatial
961 learning. Behav Neurosci 113:1189-1203.

962 Santín LJ, Aguirre JA, Rubio S, Begega A, Miranda R, Arias JL (2003) c-Fos expression
963 in supramammillary and medial mammillary nuclei following spatial reference and
964 working memory tasks. Physiol Behav 78:733-739.

965 Saper CB (1985) Organization of cerebral cortical afferent systems in the rat. II.
966 Hypothalamocortical projections. J Comp Neurol 237:21-46.

967 Sapin E, Lapray D, Bérod A, Goutagny R, Léger L, Ravassard P, Clément O, Hanriot L,
968 Fort P, Luppi PH (2009) Localization of the brainstem GABAergic neurons controlling
969 paradoxical (REM) sleep. PLoS One 4:e4272

970 Sasaki T, Leutgeb S, Leutgeb JK (2015) Spatial and memory circuits in the medial
971 entorhinal cortex. Curr Opin Neurobiol 32:16-23

972 Schmidt B, Marrone DF, Markus EJ (2012) Disambiguating the similar: the dentate
973 gyrus and pattern separation. Behav Brain Res 226:56-65.

974 Segal M, Landis S (1974) Afferents to the hippocampus of the rat studied with the
975 method of retrograde transport of horseradish peroxidase. *Brain Res* 78:1-15.

976 Shahidi S, Motamedi F, Naghdi N (2004) Effect of reversible inactivation of the
977 supramammillary nucleus on spatial learning and memory in rats. Brain Res 1026: 267-
978 274.

979 Soussi R, Boulland JL, Bassot E, Bras H, Coulon P, Chaudhry FA, Storm-Mathisen J,
980 Ferhat L, Esclapez M (2015) Reorganization of supramammillary–hippocampal
981 pathways in the rat pilocarpine model of temporal lobe epilepsy: evidence for axon
982 terminal sprouting. Brain Struct Funct 220: 2449-2468.

983 Soussi R, Zhang N, Tahtakran S, Houser CR, Esclapez M (2010) Heterogeneity of the
984 supramammillary-hippocampal pathways: evidence for a unique GABAergic
985 neurotransmitter phenotype and regional differences: GABAergic and glutamatergic
986 supramammillary-hippocampal pathways. Eur J Neurosci 32:771-785.

987 .Swanson LW (1982) The projections of the ventral tegmental area and adjacent regions:
988 a combined fluorescent retrograde tracer and immunofluorescence study in the rat.
989 Brain Res Bull 9:321-353.

990 Swanson LW (1998) Brain Maps: Structure of the Rat Brain. Elsevier, Amsterdam

991 Ugolini G (2010) Advances in viral transneuronal tracing. J Neurosc Methods 194:2-20.

992 Vertes RP (1992) PHA-L analysis of projections from the supramammillary nucleus in
993 the rat. *J Comp Neurol* 326:595-622.

994 Vertes RP (2015) Major diencephalic inputs to the hippocampus. *Prog Brain Res*
995 121:144.

996 Vertes RP, Kocsis B (1997) Brainstem-diencephalo-septohippocampal systems
997 controlling the theta rhythm of the hippocampus. Neuroscience 81:893-926.

998 Vertes RP, McKenna JT (2000) Collateral projections from the supramammillary nucleus
999 to the medial septum and hippocampus. Synapse 38:281-293.

1000 Wyss JM, Swanson LW, Cowan WM (1979) A study of subcortical afferents to the
1001 hippocampal formation in the rat. Neuroscience 4:463-476.

1002 Zhang N, Houser CR (1999) Ultrastructural localization of dynorphin in the dentate gyrus
1003 in human temporal lobe epilepsy: a study of reorganized mossy fiber synapses. J Comp
1004 Neurol 405:472-490.

1005

1006

1006 **Figures**

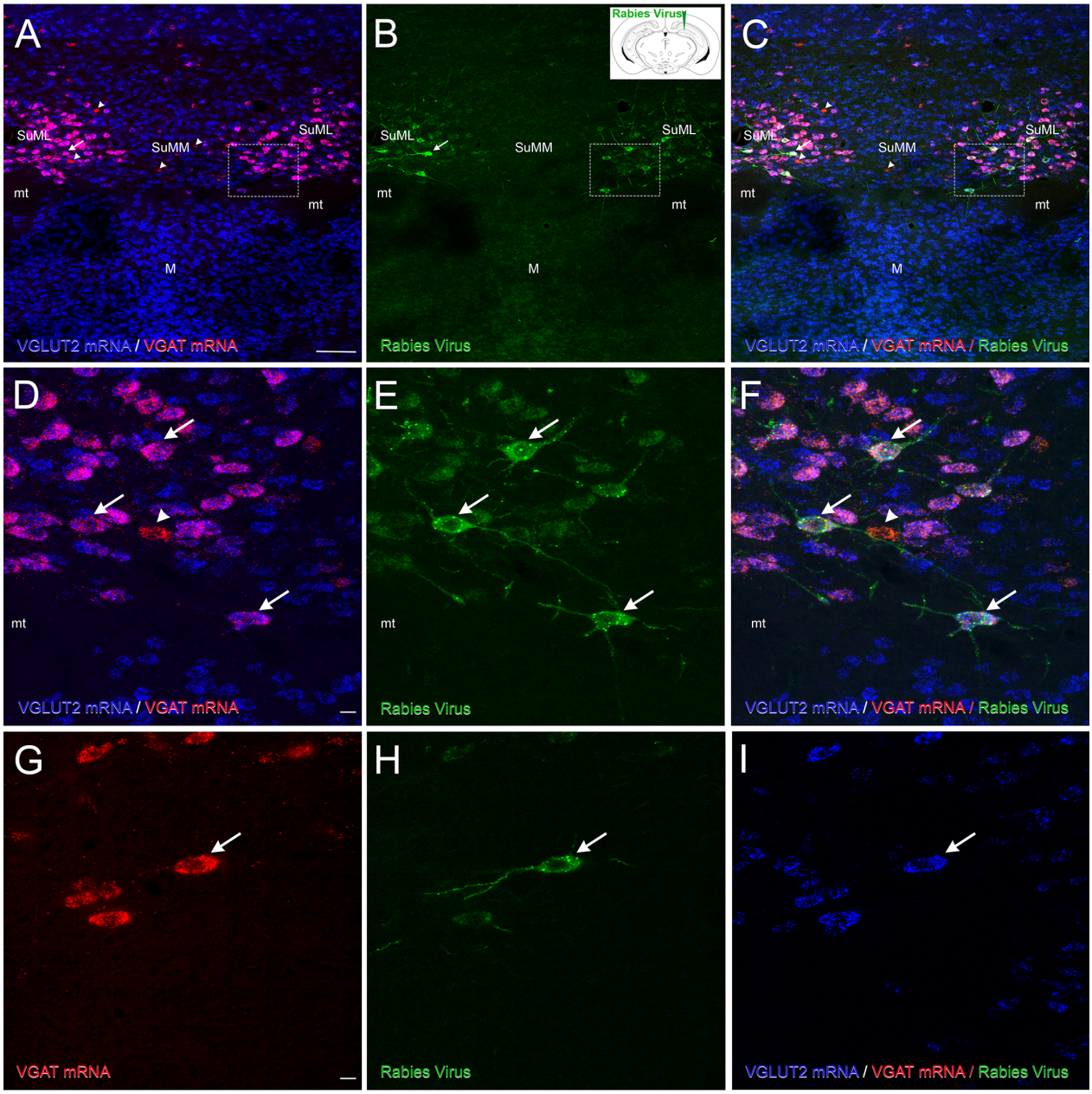

1007

1008 **Figure 1: Neurochemical features of SuML neurons innervating the dorsal dentate**
1009 **gyrus (DG) characterized by simultaneous labeling for the rabies virus (RV)**
1010 **retrograde tracer (green), VGAT mRNA (red) and VGLUT2 mRNA (blue) in a**
1011 **coronal section.**

1012 (A-I) All confocal images were obtained from sequential acquisition of separate
1013 wavelength channels, corresponding to the different fluorophores used for the triple
1014 labeling, from a single optical slice. This optical slice was acquired in the
1015 supramammillary region of the hypothalamus from a coronal section of a VGLUT2-cre
1016 mouse that received an injection of RV in supragranular layer of the DG (B, insert). A)
1017 Image obtained from the merge of the two confocal images corresponding respectively
1018 to the labeling of VGLUT2 (blue) and VGAT (red) mRNAs. Many neurons expressing
1019 both VGLUT2 and VGAT mRNAs (arrow) were observed in the lateral region of the
1020 supramammillary nucleus (SuML). They were located almost exclusively above and
1021 around the mammillary tract (mt). Neurons expressing VGLUT2 mRNA only (blue) were
1022 observed mainly in the most medial part of the SuM (SuMM) and were numerous in the
1023 mammillary nucleus (M). Few neurons containing VGAT mRNA only (red, arrowheads)
1024 were distributed in the SuML and SUMM. B) Confocal image corresponding to the
1025 immunohistochemical labeling of the RV (green) showing that all RV containing neurons
1026 in the SuM were located in the region of the SuML surrounded the mt. C) Merge of A-B.
1027 (D-F) Higher magnification of region outlined in A-C showing that all these SuML
1028 neurons projecting to the DG, labeled for the RV (E, arrows), co-expressed VGLUT2 and
1029 VGAT mRNAs (D, F, arrows). (G-I) RV labeled neuron (H, arrow) co-expressed VGAT
1030 mRNA (G, arrow) and VGLUT2 mRNA (I, arrow) Scale bars: A-C, 100μm; D-I, 10μm.
1031

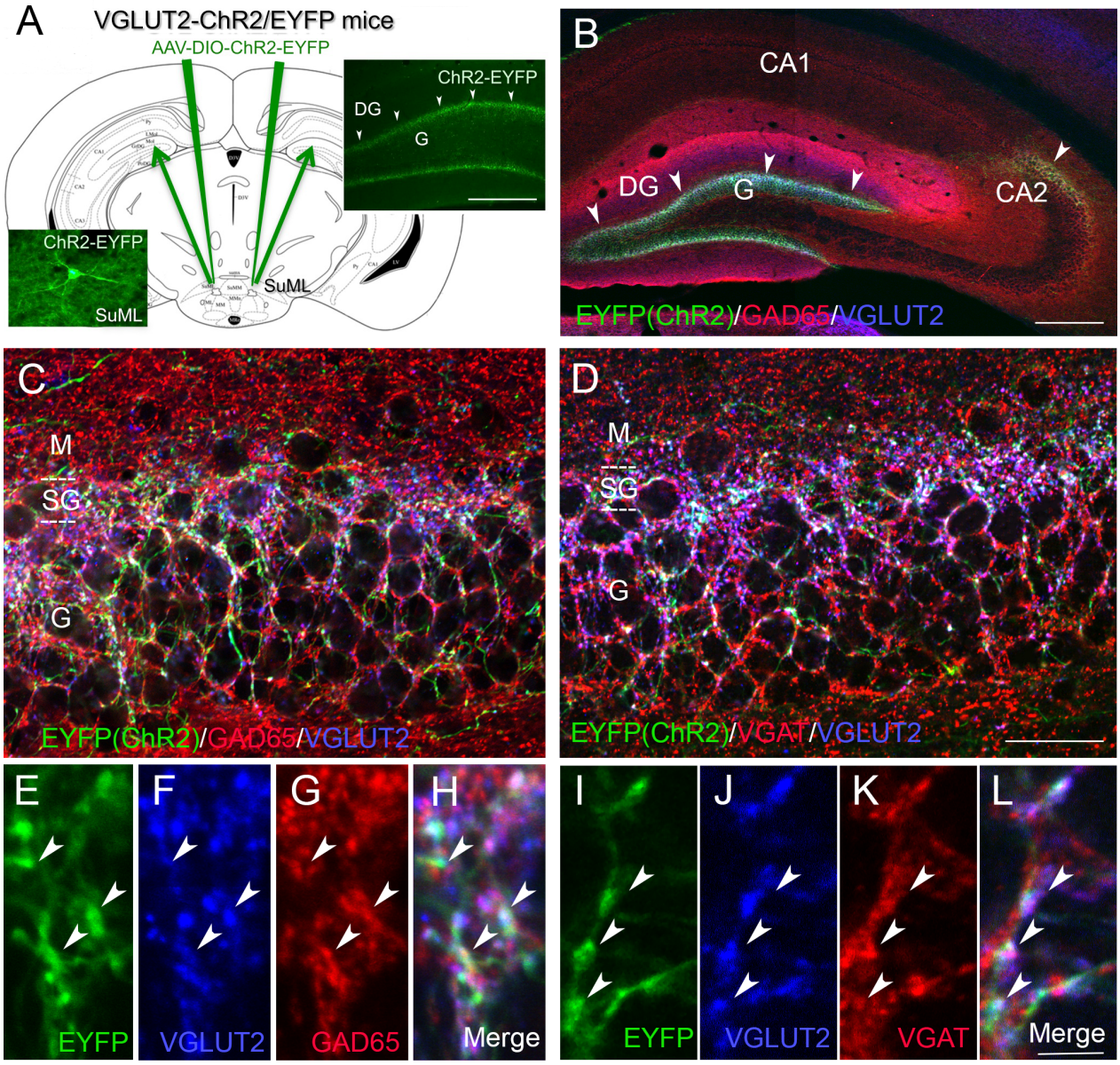

Figure 2: Neurochemical features of axon terminals from SuML neurons innervating the dorsal DG characterized by simultaneous immunohistochemical labeling for the AAV-EYFP anterograde tracer (green), GAD65 or VGAT (red) and VGLUT2 (blue) in coronal sections.

(A) Diagram illustrating the bilateral injections of the viral vector AAV-DIO-ChR2-EYFP within the lateral region of the SuM. Images from a coronal section showing endogenous fluorescence of EYFP observed in the cell body and proximal dendrites of a transfected

1040 neuron located within the SuML as well as fibers and axon terminals within the
1041 supragranular (arrowheads) and granular layer (G) of the DG. (B) Image obtained from a
1042 single optical slice showing labeling for EYFP (green), GAD65 (red) and VGLUT2 (blue)
1043 in the hippocampus. Fibers labeled with the anterograde tracer AAV-DIO-ChR2-EYFP
1044 injected within the SUM as illustrate in (A) were exclusively located in the supragranular
1045 (arrowheads) and granule cell (G) layers as well as the CA2 region of the hippocampus.
1046 (C, D) Images corresponding to a maximum intensity z-projection of a stack of 8 optical
1047 slices spaced at 370 nm, showing labeling for EYFP (green), VGLUT2 (blue) and
1048 GAD65 (C, red) or VGAT (D, red) in the dorsal DG. Axon terminals and fibers, from
1049 neurons in the SuML, labeled for the EYFP anterograde tracer (green) were located
1050 mainly in the supragranular layer but also in the granule cell layer. Numerous GAD65-
1051 (C) or VGAT- (D) containing terminals were present in the molecular layer (M) and
1052 granule cell layer (G) of the dorsal DG. VGLUT2-containing terminals were mainly
1053 located in the supragranular layer (SG) but were also observed in G. (E–L) Images of
1054 the three different fluorophores used for the triple labeling, obtained by sequential
1055 acquisition of separate wavelength channels from a single optical slice, in the SG of the
1056 DG demonstrated that many if not all axon terminals labeled for EYFP (B, I, green,
1057 arrowheads) contained GAD65 (G, red arrowheads), VGAT (K, red, arrowheads) but
1058 also VGLUT2 (F, J blue, arrowheads). (H) Merge of E-G. (L) Merge of I-K. Scale bars: A-
1059 B, 200μm; C-D, 25μm and E-L, 3μm.
1060

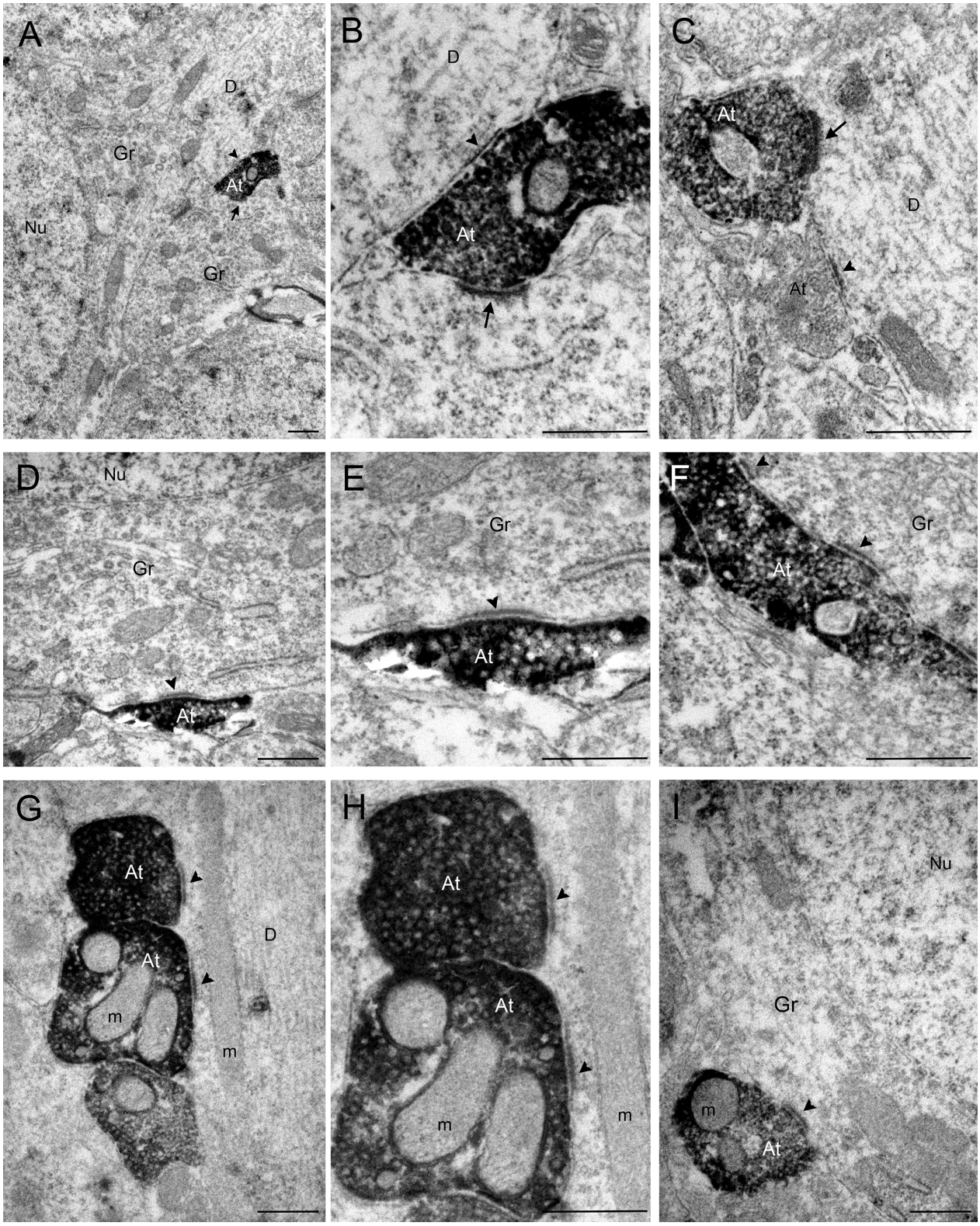

1061

1062 **Figure 3: Pre-embedding immunolabeling for EYFP anterograde tracer in ultrathin**

1063 **coronal sections of the dorsal DG.**

1064 (A–I) In the dorsal DG, numerous axon terminals were labeled for EYFP, revealed by
1065 electron-dense peroxidase 3.3'-diaminobenzidine tetrahydrochloride product. (A) A
1066 labeled axon terminal (At) making two synaptic contacts (arrow and arrowhead) on
1067 unlabeled somata of 2 presumed granule cells (Gr). (B) Higher magnification of the At
1068 illustrated in (A) showing that these two synaptic contacts were different: one displayed
1069 a relatively thin post-synaptic densities (arrowhead) characteristic of symmetric
1070 synapses on the soma of one Gr; the other one displayed a thick post-synaptic densities
1071 (arrow) characteristic of asymmetric synapses on the soma of another Gr. (C) Labeled
1072 axon terminals established synaptic contacts displaying a thick synaptic densities on
1073 unlabeled dendritic processes (D) that differed from the synaptic contact formed by the
1074 unlabeled At (arrow). The synaptic contacts illustrated in D-I displayed relatively thin
1075 post-synaptic densities (arrowheads) on the soma (D-F, I) or dendrites (G, H) of
1076 unlabeled Gr. m, mitochondria; Nu, nucleus. Scale bar: A-I, 0.5 μm.
1077

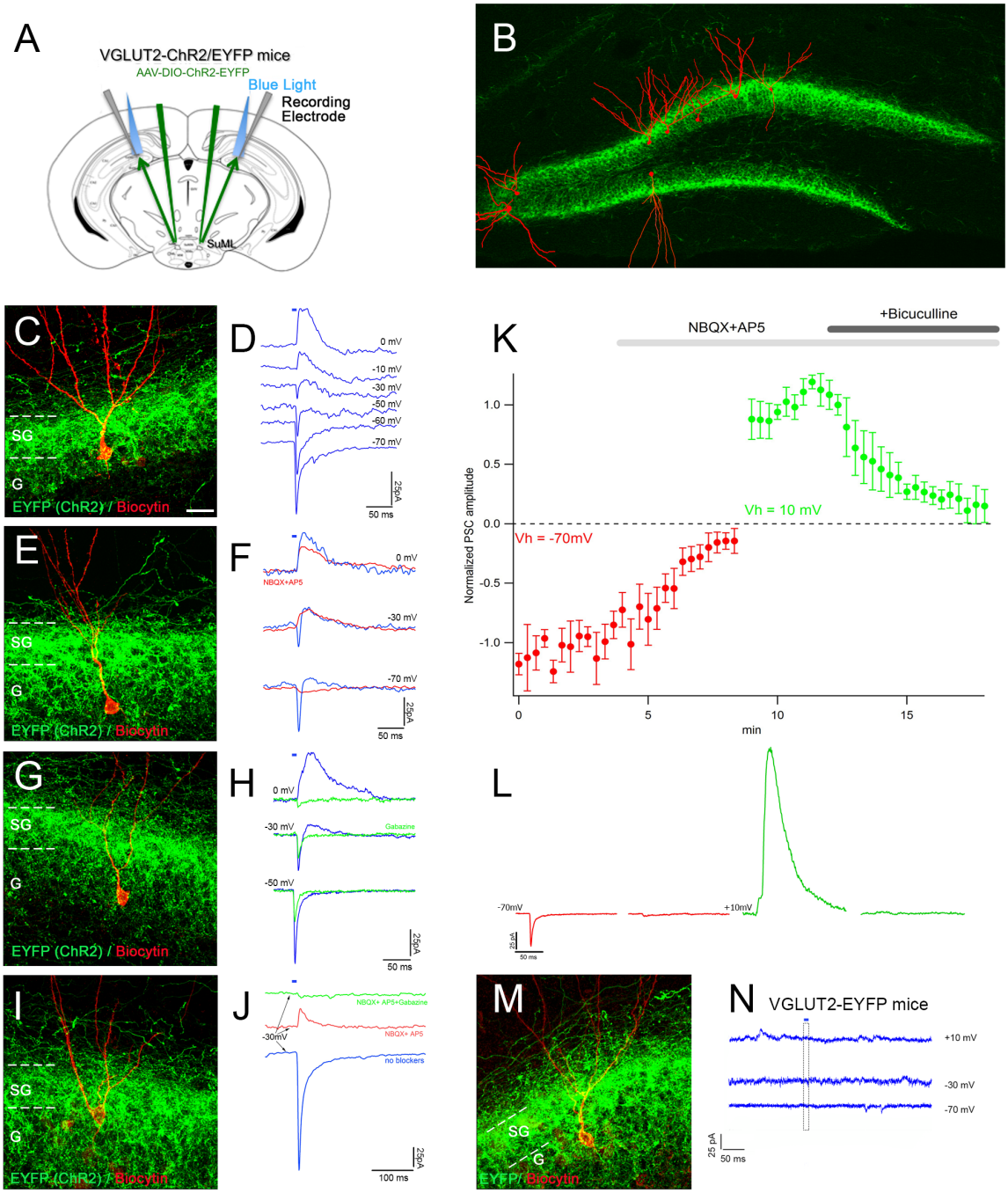

1078

1079 **Figure 4: Selective stimulation of axonal terminals from SuML neurons**
1080 **innervating the dorsal DG, performed in hippocampal slices of VGLUT2-ChR2-**
1081 **EYFP mice, induced co-release of GABA and glutamate on DG granule cells.**

1082 (A) Diagram illustrating the site of the bilateral injections of AAV-DIO-ChR2-EYFP in
1083 VGLUT2-cre mice, of light stimulations and of the recorded patch clamp electrode in the
1084 DG of the VGLUT2-ChR2-EYFP mice. (B) Montage illustrating the position within the
1085 dentate granule cell layer of the biocytin-filled cells reconstructed after patch clamp
1086 recordings and EYFP-labeled terminals originating from SuML neurons.
1087 (D, F, H, J, N) Examples of light induced PSCs recorded in DG cells illustrated in (C, E,
1088 G, I, M). (D) Light induced post-synaptic currents (PSCs) recorded at different holding
1089 potentials in DG neuron; short black bar above the upper trace shows the time moment
1090 and duration of light stimulus. Note at -70 mV to -50 mV holdings the PSCs had
1091 negative-going direction (inward) currents. They were positive-going (outward) at -10 mV
1092 and 0 mV but displayed both negative- and positive-going phases when the neuron
1093 membrane was clamped at -30 mV. This suggests that light stimulation induces two
1094 types of postsynaptic currents. Indeed, the application of glutamate receptor blockers
1095 NBQX and AP5 (F, red traces) inhibited inward (F, negative going) component of PSCs
1096 recorded at negative holding potentials (Vh), but had only small effect on outward
1097 component (positive going) recorded at positive Vh. Inversely, the outward component of
1098 light induced PSCs was sensitive to GABA A receptor inhibitor gabazine (H, green vs
1099 blue traces). This suggests that these PSCs are generated by simultaneous activation of
1100 glutamate and GABA post-synaptic receptors. Interestingly at -50 mV holding, PSC was
1101 larger without gabazine (H, blue versus green trace), probably because GABA-mediated
1102 current hyperpolarizes the membrane potential increasing thus the driving force for the
1103 glutamatergic current. In voltage-clamp condition such an interaction is possible if the
1104 pool of postsynaptic GABA Rs is close to the postsynaptic Glu R pool. (K, L) Effect of
1105 glutamate and GABA A receptors blockers on the peak amplitude of light pulse evoked

1106 PSC recorded at -70 mV (red circles) and 10 mV (green circles) holding potentials. For
1107 each Vh the peak amplitudes of first 10 PSCs were averaged and used then as a
1108 normalization factor for all peak amplitude recorded at given potential. Each point and
1109 error bars corresponds the mean ± SD of PSC normalized amplitude recorded in 5 DG
1110 neurons. In regular ACSF the repetitive light pulses (5 ms, 0.05 Hz) evoked PCS of
1111 relatively stable amplitude (1.00 ± 0.26, L left hand side red trace-an example of
1112 averaged response of one neuron). The application of glutamate receptor blockers (10
1113 μM NBQX + 40 μM D-AP5) reduced the peak amplitude by 84% (0.16 ± 0.15, $p<0.01$,
1114 n= 5, paired Wilcoxon test). The remaining response was seen in 4 from 5 neurons and
1115 is probably due to GABA A mediated current because at -70 mV the driving force for
1116 chloride driven currents is close to but not zero (L, red trance in the middle) therefore in
1117 case of GABA massive release some inward current is still possible. Indeed a switch to
1118 Vh= 10 mV revealed a huge PSC response to light stimulation (L, green trace in the
1119 middle) which amplitude was stable (1.00 ± 0.20) but progressively reduced to 12%
1120 (0.12 ± 0.16, $p<0.01$, n= 5, paired Wilcoxon test) by the addition of 10 μM bicuculline to
1121 the ACSF already containing GluR blockers (L, green trace at left). In 3 from 5 neurons,
1122 6 min lasting bicuculline application completely abolished response to light pulses. In
1123 two neurons the remaining current is probably due to the competitive character of
1124 bicuculline induced inhibition i.e in case of high GABA release 10 μM of bicuculline may
1125 be not sufficient to all receptors inhibition. (M, N) The identical light stimulation (5 ms,
1126 10%, 50% 90% max power LED) of fibers and axon terminals expressing EYFP on
1127 slices of control VGLUT2-EYFP mice (n= 3) did not evoke any response in the recorded
1128 granule cells (n= 5) confirming that ChR2 activation is required to obtain the PSCs.
1129 Scale Bar: C, E, G, I, M, 20μm.

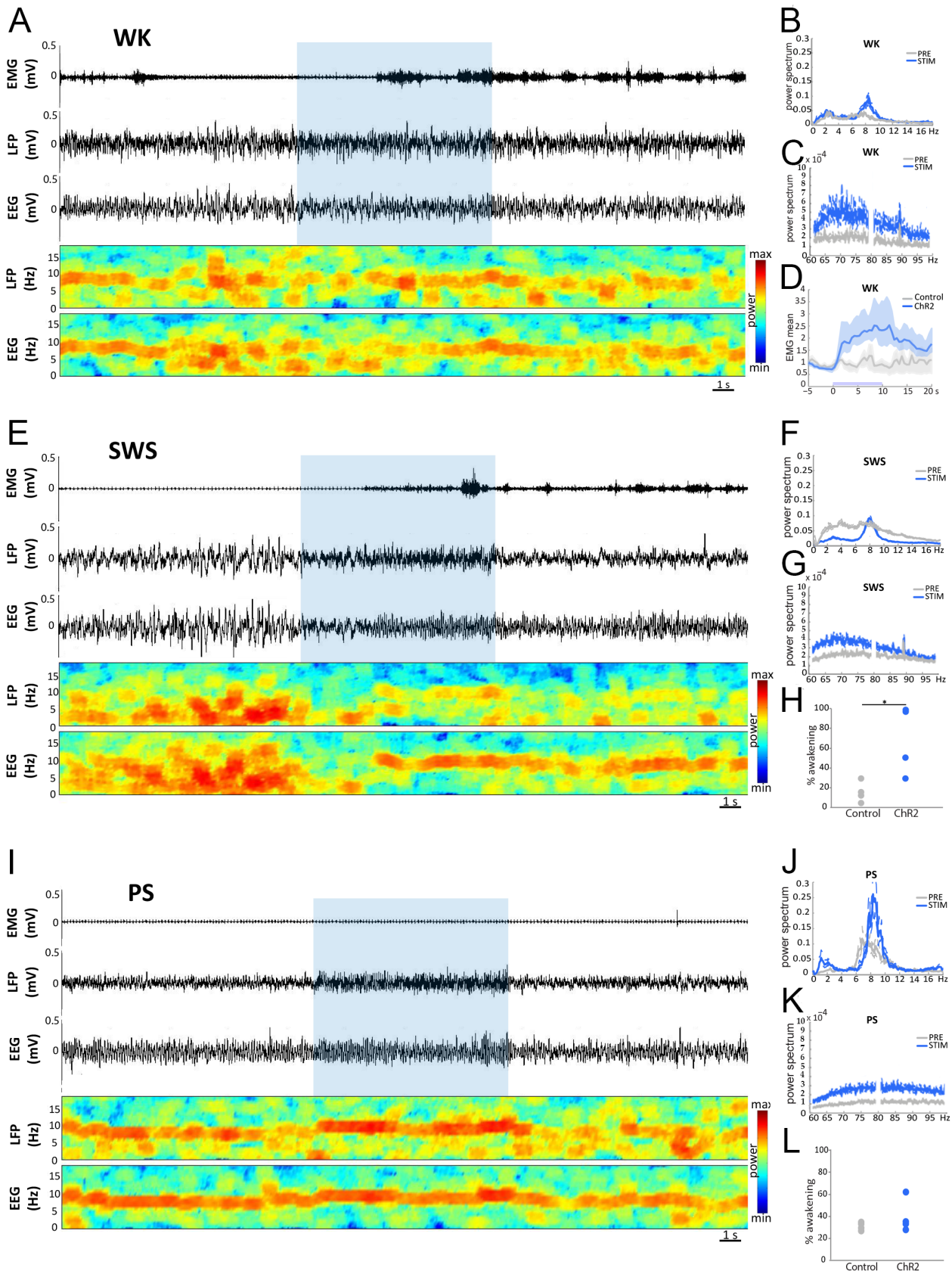
A
WK
EMG (mV)
LFP (mV)
EEG (mV)
LFP (Hz)
EEG (Hz)
max
power
min
1 s
B
WK
PRE
STIM
power spectrum
C
WK
PRE
STIM
power spectrum
D
WK
Control
ChR2
EMG mean
E
SWS
EMG (mV)
LFP (mV)
EEG (mV)
LFP (Hz)
EEG (Hz)
max
power
min
1 s
F
SWS
PRE
STIM
power spectrum
G
SWS
PRE
STIM
power spectrum
H
% awakening
Control
ChR2
I
PS
EMG (mV)
LFP (mV)
EEG (mV)
LFP (Hz)
EEG (Hz)
max
power
min
1 s
J
PS
PRE
STIM
power spectrum
K
PS
PRE
STIM
power spectrum
L
% awakening
Control
ChR2

1130

Figure 5: Effects of light stimulation of axonal terminals from SuML neurons innervating the dorsal DG on DG LFP, EEG recordings and behavior of VGLUT2-ChR2-EYFP mice during WK, SWS and PS.

(A, E, I) Examples of raw recording for EMG, LFP recorded in the DG and parietal cortex EEG as well as associated time-frequency analysis of LFP and EEG in a VGLUT2-ChR2-EYFP mouse during WK (A), SWS (E) and PS (I). The blue bar represents the optogenetic stimulation period (20 Hz with pulses of 10 ms for 10 s). (B, C, F, G, J, K) LFP power spectra between 0-18 Hz and 60-100 Hz in VGLUT2-ChR2-EYFP mouse before and during light stimulation (20 Hz 10 s, pulses of 10 ms, during 4 h) during WK (B, C), SWS (F, G) and PS (J, K). An effect was clearly visible on the LFP in all vigilance states. The stimulation induced a slight increase in the theta power during WK (A, B) and a major increase in theta power and frequency during PS (I, J) as well as a clear reduction of slow waves oscillation during SWS (E, F). The stimulation during WK and PS also increased the power of gamma (C, K). Light stimulation during WK increased locomotor activity reflected by an increase of EMG signal in VGLUT2-ChR2-EYFP mice (A, D, blue trace) as compared to control VGLUT2-EYFP mice (D, grey trace). (H) Light stimulation during SWS induced awakening reflected by a significant increase of the awakening percentage after stimulation in most VGLUT2-ChR2-EYFP mice (range 30% to 100%) as compared to that observed in control VGLUT2-EYFP mice (range: 0% to 30 %). (L) In contrast no significant difference in the percentage of awakening was observed between VGLUT2-CHR2-EYFP and control VGLUT2-EYFP mice when stimulation was performed during PS.

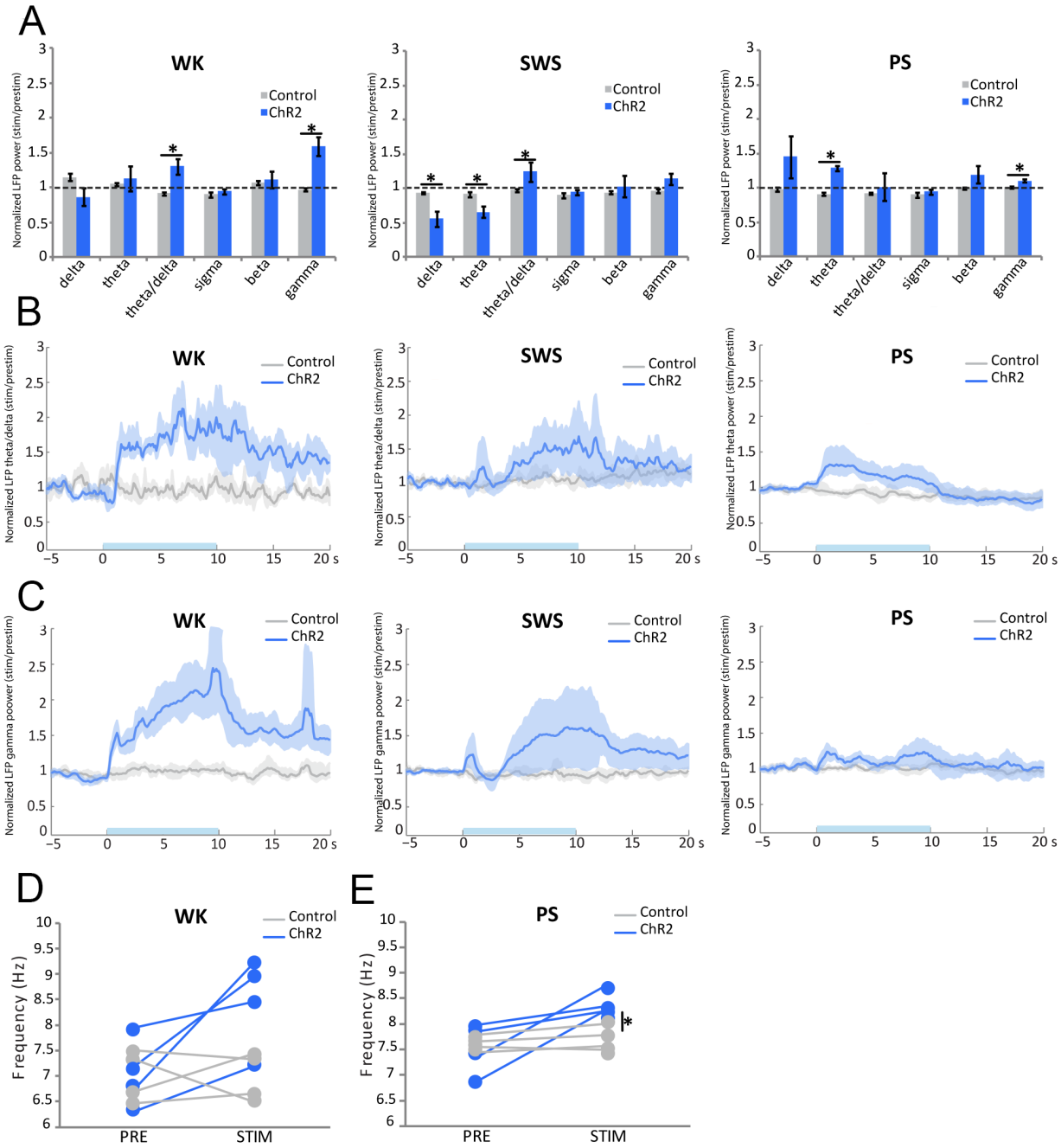

Figure 6: Comparison of the effects of light stimulation of axonal terminals from SuML neurons innervating the dorsal DG on DG LFP performed during WK, SWS and PS between VGLUT2-ChR2-EYFP and control VGLUT2-ChR2-EYFP mice.

(A) Ratio of power recorded during light stimulation to that recorded before the stimulation (20 Hz, 10 s for 4 h with pulses 10 ms) for the different frequency bands

(delta, theta, gamma) of LFP in VGLUT2-ChR2-EYFP (n= 4) and control VGLUT2-EYFP (n= 4) mouse groups during WK, SWS and PS. These ratios illustrate: an increased power in the theta frequency band during stimulations performed in PS; an increase of theta/delta power during the stimulation when performed in WK and SWS and an increased power in the gamma frequency band when stimulations were performed during WK and PS in the VGLUT2-ChR2-EYFP group. Increased power observed during stimulations observed in the ChR2 group differed significantly from random variation observed before and after the stimulation in the control group. Significance: Mann Whitney: * $p < 0.05$. (B, C) Theta/delta (B) and gamma (C) power ratios as a function of time after light stimulation during the different vigilance states. The blue bar on the x axis represents the stimulation period. Shaded regions show 95% confidence intervals. During WK, a significant increase of theta/delta (B) and gamma (C) power occurred in VGLUT2-ChR2-EYFP group immediately after the light stimulation. These increases were observed during the entire 20 s period analyzed. The increase of theta/delta during SWS occurred two to three seconds after the stimulation. The increase of theta (B) and gamma (C) powers during PS occurred immediately after the stimulation and stayed during the 10 s period of stimulation. No difference induced by the stimulation was observed in the control group. (D, E) Peak frequency analysis of theta before and during optogenetic stimulation in the control group (n= 4) and the ChR2 group (n= 4). Significance: Mann Whitney, * $p < 0.05$ compared to the control group.

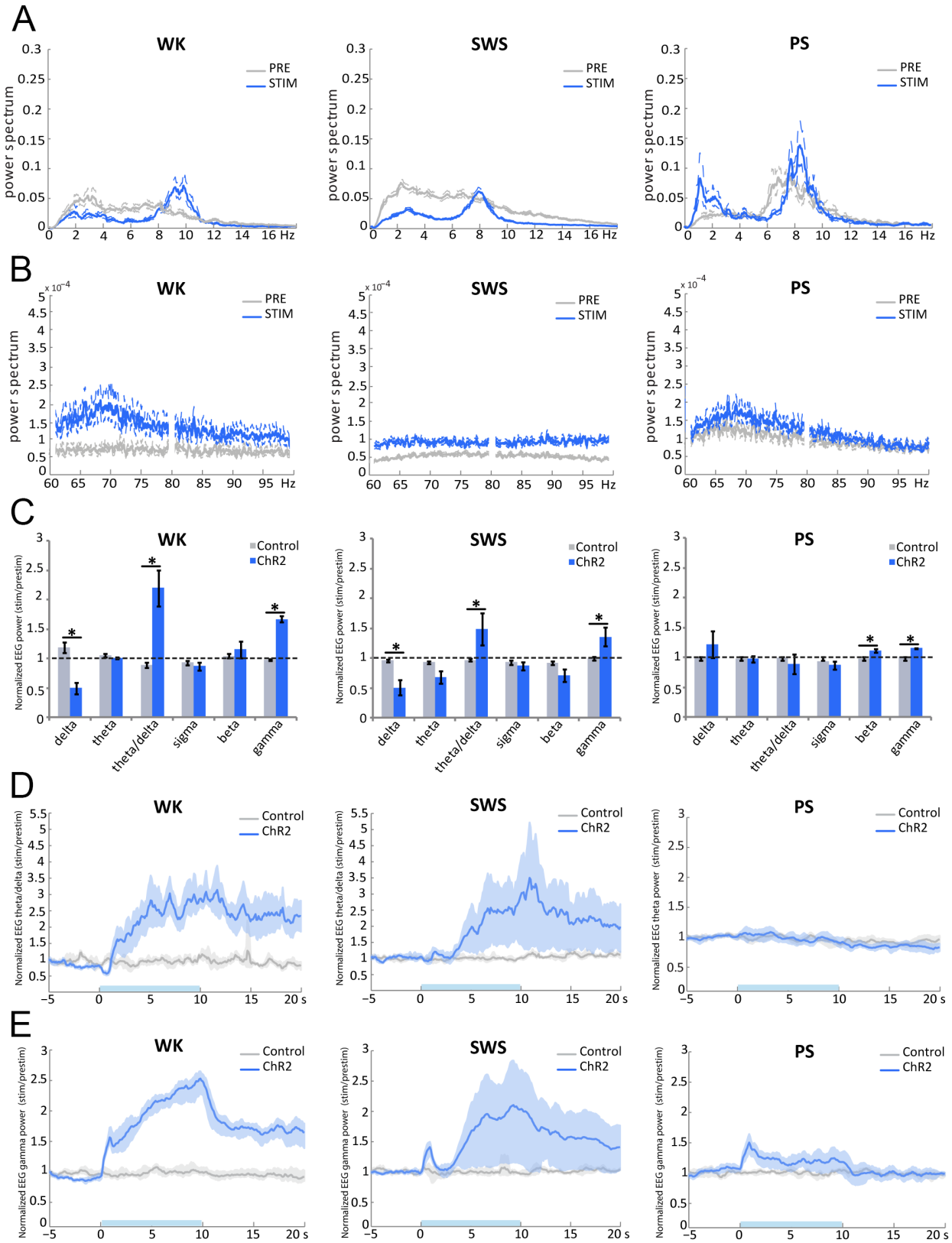
A
WK
SWS
PS
PRE
STIM
power spectrum
Hz
B
x 10^-4
C
Control
ChR2
Normalized EEG power (stim/prestim)
delta
theta
theta/delta
sigma
beta
gamma
D
Normalized EEG theta/delta (stim/prestim)
Normalized EEG theta power (stim/prestim)
s
E
Normalized EEG gamma power (stim/prestim)

1182

1183 **Figure 7: Comparison of the effects of light stimulation of axonal terminals from**
1184 **SuML neurons innervating the dorsal DG on EEG performed during WK, SWS and**
1185 **PS between VGLUT2-ChR2-EYFP and control VGLUT2-EYFP mice.**
1186 (A, B) EEG power spectra between 0-18 Hz and 60-100 Hz in a VGLUT2-ChR2-EYFP
1187 mouse before and during light stimulation (20 Hz 10 s, pulses of 10 ms, during 4 h)
1188 during WK, SWS and PS. An effect was clearly visible on the EEG in all vigilance states.
1189 (C) Ratio of power recorded during light stimulation to that recorded before the
1190 stimulation for the different frequency bands (delta, theta, gamma) of EEG in VGLUT2-
1191 ChR2-EYFP (n= 4) and control VGLUT2-EYFP (n= 4). These ratios illustrate an increase
1192 of theta/delta power during the stimulation when performed in WK and SWS and an
1193 increased power in the gamma frequency band when stimulations were performed
1194 during all vigilance states in the VGLUT2-ChR2-EYFP group. These increased powers
1195 during stimulations observed in ChR2 group differed significantly from random variation
1196 observed before and after the stimulation in the control group. Significance: Mann
1197 Whitney: * $p < 0.05$. (D, E) Theta/delta (D) and gamma (E) power ratios as a function of
1198 time after light stimulation during the different vigilance states. The blue bar on the x axis
1199 represents the stimulation period. Shaded regions show 95% confidence intervals.
1200 During WK, a significant increase of theta/delta (B) and gamma (C) powers occurred in
1201 VGLUT2-ChR2-EYFP group immediately after the light stimulation. These increases
1202 were observed during the entire 20 s period analyzed. The increase of theta/delta during
1203 SWS occurred two to three seconds after the stimulation. The increase of gamma (C)
1204 powers during PS occurred immediately after the stimulation and lasted during the 10 s
1205 period of stimulation. No increase in theta was observed during PS (C, D) in the EEG.
1206 No difference induced by the stimulation was observed in the control group.

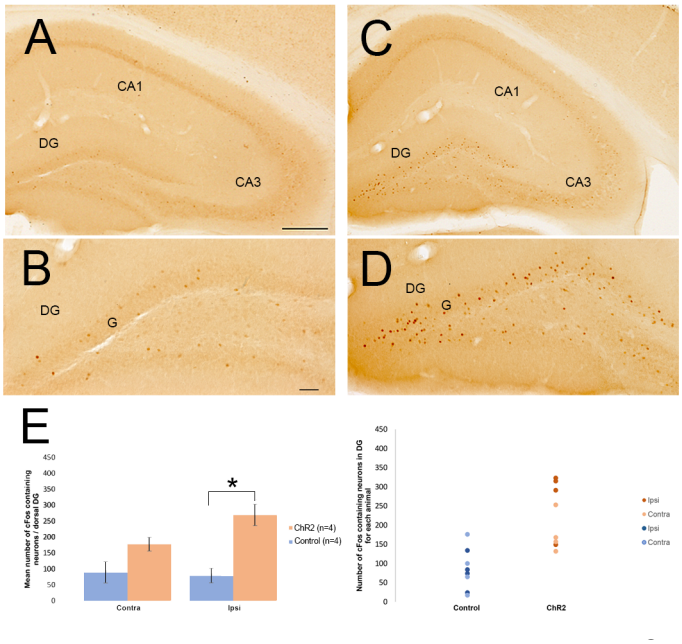

Figure 8: Activation of DG cells after light stimulation of axon terminals from SuML neurons innervating the DG in VGLUT2-ChR2-EYFP and VGLUT2-EYFP as reflected by cFos immunohistochemical labeling. (A, B, C, D) Immunohistochemical labeling for cFos on sections of control VGLUT-EYFP (A, B,) and VGLUT2-ChR2-EYFP (C, D) mice. In control mice (A, B) only very few neurons labeled for cFos were observed in the hippocampus. There were scattered in all layers of the hippocampus including CA1, CA3 and the DG. In addition, these neurons were lightly labeled for cFos including in the granule cell layer (G) of the DG. In contrast, in VGLUT2-ChR2-EYFP mice, many c-Fos containing neurons were located in the granule cells layer (G) of the DG whereas only a few were observed within the CA3 and CA1 regions of the hippocampus. In the granule cell layer these neurons were highly labeled for cFos (D) as compared to those observed in control mice (B). (E) Quantitative analysis confirmed a clear increase number of cFos-containing neurons in the granule cell layer of the DG stimulated (ipsi) but not in the contralateral DG (contra) in VGLUT2-ChR2-EYFP mice (n= 4) as compared to control mice (n= 4). Wilcoxom Rank Sum test * P< 0.05%; Scale Bars: A, C: 250 µm; B, D: 50 µm.